

FIGURE 1. Surface marker and cytokine expression in naive and Ag-specific effector and memory CD4⁺ T cells. Splenic CD4⁺ T cells from DO11.10-Tg mice were stimulated with an OVA323–339 peptide plus APC for 5 d in vitro, resulting in Ag-specific effector cells, followed by transfer into normal syngeneic BALB/c recipient mice to generate memory cells. **(A)** Surface markers on CD4⁺ T cells (double positive for KJ1 and CD4, upper left panel) were analyzed by flow cytometry. **(B)** IFN- γ , IL-4, and TNF- α production by naive, effector, and memory CD4 T cells was assessed by intracellular cytokine staining.

Real-time PCR

cDNA was prepared from total RNA samples using an Applied Biosystems (Foster City, CA) cDNA Archive Kit and random primers. The assay was run in triplicate for each RNA sample, in accordance with the manufacturer's recommendations, with each reaction containing 50 ng total cDNA (as total input RNA) per 20- μ l reaction volume. The cycling conditions for SYBR Green dye I quantitative real-time PCR with 2 \times Applied Biosystems Universal Master Mix were 2 min at 50°C, 10 min at 95°C, followed by 40 rounds of 15 s at 95°C and 1 min at 60°C, with analysis by an Applied Biosystems 7500 PCR system. β -actin was used as the reference gene. Primer sequences are listed in Supplemental Table I. Data acquisition and analysis were performed using SDS 2.1 software in relative quantity mode, with each sample analyzed three times. After PCR, CT values were determined and used to calculate normalized $2^{-\Delta\Delta CT}$ values.

Luciferase reporter assay

Fragments of DMRs of the mouse *Nr1D1*, *Ptgir*, *Tnfrsf4*, *Tbx21*, *Cish*, *Chsy1*, *Sdf4*, *Hps4*, *Sema4d*, *Mtss1*, *Klf7*, *Wdfy2*, *Nr5a1*, and *MapK1lip1* loci were amplified by PCR using genomic DNA as a template and the primers shown in Supplemental Table I. To generate a luciferase reporter vector on a CpG-free background, the 500–800-bp PCR product was inserted into the pCpGL-CMV/EF1 vector (a gift from Dr. M. Rehli and Dr. M. Klug) using the In-Fusion cloning system (Clontech), replacing the CMV enhancer with the DMR regions (19).

The luciferase reporter vector pCpGL-Cish-DMR/EF1 was methylated in vitro using methylase SssI (New England BioLabs), according to the manufacturer's instructions, followed by purification using a QIAquick PCR clean-up kit. In control samples using pCpGL-EF1 and pCpGL-Cish-DMR/EF1, the methyl-group donor S-adenosylmethionine was omitted. Successful methylation of the reporter plasmid containing the DMR was verified by reaction with the methylation-sensitive and methylation-resistant enzymes HpaII and MspI, respectively.

EL-4 T cells (5×10^6 cells) were transfected with 2.5 μ g either methylated or unmethylated pCpGL-DMR/EF1 vector or using a control plasmid with no insert, in triplicate. Synthetic *Renilla* luciferase reporter vector (pRL-TK; Promega) was cotransfected (1.5 μ g) and served as an internal control for efficiency. EL-4 cells were electroporated with a Bio-Rad Gene Pulser at 270 V and a capacitance of 975 μ F. Twelve hours later, transfected cells were stimulated with PMA (50 ng/ml) and ionomycin (0.5 μ g/ml) for 16 h. The cells were harvested, and luciferase activity was measured by the Dual Luciferase Assay system using an Orion L luminometer. Firefly raw light unit data were normalized to *Renilla* luciferase activity and expressed relative to the control vector with no insert.

Gene ontology

Gene ontology was estimated using Gostat software (25).

Table I. Genome-wide methylation sequencing summary for CD4⁺ T cell DNA cut with HpaII or MspI restriction nuclease

| Cell Type | Nuclease | No. of Hits in Genome | Unique Tags ^a | % |
|-----------|----------|-----------------------|--------------------------|----|
| Naive | HpaII | 9,902,632 | 5,074,880 | 51 |
| | MspI | 12,994,381 | 5,499,474 | 42 |
| Effector | HpaII | 9,349,718 | 6,039,406 | 65 |
| | MspI | 9,673,142 | 6,140,353 | 63 |
| Memory | HpaII | 13,582,273 | 7,055,612 | 52 |
| | MspI | 9,943,128 | 4,193,004 | 42 |
| Total | | 65,445,274 | 34,002,729 | 52 |

Twenty-base pair MSCC tags were mapped in the genome.

^aNumber of tags in restriction sites for analysis of DNA methylation.

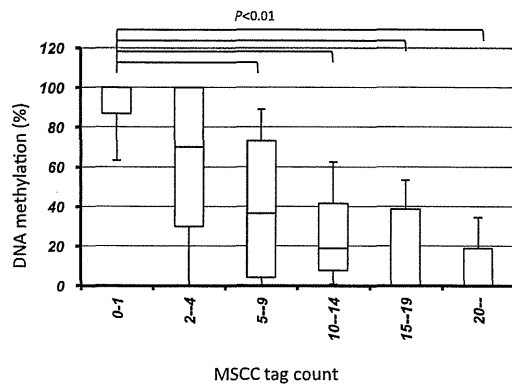


FIGURE 2. The relationship between MSCC tag counts and bisulfite sequencing data. To validate the methylation levels determined by MSCC, we designed primers targeting 130 profiled locations in bisulfite-treated DNA and performed PCR amplification and Sanger sequencing of the PCR product. Horizontal lines represent median methylation as determined by bisulfite sequencing, boxes represent the quartiles, and whiskers mark the 5th and 95th percentiles. $p < 0.01$, Kruskal–Wallis H test.

Bisulfite sequencing

Bisulfite sequencing was performed to verify SOLiD data. Bisulfite modification of genomic DNA was performed using the EpiTect Bisulfite Kit (QIAGEN). We used Methyl Primer Express software (Applied Biosystems) to design primers. Bisulfite-treated DNA was amplified by PCR. The PCR products were cloned into the pCR2.1-TOPO vector and transformed into One Shot TOP10 Competent Cells (Invitrogen). At least 24 clones were sequenced using an ABI3730 Sequencer. The data were analyzed using QUMA, a quantification tool for methylation analysis (Riken Institute of Physical and Chemical Research, Yokohama, Japan).

Statistical analysis

Comparisons of each 5'-end tag were performed using Z-test statistics (24).

Accession number

5'-end and MSCC tags have been deposited in the National Center for Biotechnology Information Sequence Read Archive (<http://www.ncbi.nlm.nih.gov/sra>) under accession number SRP007816.

Results

Isolation of Ag-specific memory CD4⁺ T cells

To characterize memory T cells using methylome and transcriptome analysis, we generated memory CD4⁺ T cells from DO11.10 OVA-specific TCR-Tg mice. Splenic CD4⁺ T cells from the DO11.10-Tg mice were stimulated with an OVA323–339 peptide plus allophycocyanin for 5 d *in vitro* and then transferred *i.v.* into normal syngeneic BALB/c recipient mice. The transferred DO11.10-Tg T cells were monitored by staining with a clonotypic KJ1 mAb. At the time of transfer, cell surface marker expression was CD44^{high} CD127⁺ CD25⁺ CD69⁺ and CD62L⁺, but by 4 wk after cell transfer the activation markers CD25 and CD69 were no longer expressed (Fig. 1A). These observations support the development of effector and memory T cell phenotypes, respectively. To confirm the functional status of these cells, cytokine-production profiles of naive and Ag-

stimulated effector and memory cell populations were investigated. Within effector and memory T cell populations, 24 and 43%, respectively, expressed IFN- γ but not IL-4, within which 28 and 50% of cells coexpressed TNF- α (Fig. 1B).

DNA-methylation profiling in memory T cells

In this study, we used a recently developed MSCC method (23) that enables high-throughput, genome-wide identification of methylated CpG sites by SOLiD sequencing. Using the HpaII restriction nuclease, which recognizes unmethylated CCGG, most short-sequence tag fragments at HpaII cleavage sites can be uniquely mapped to genome locations. Methylation-sensitive restriction enzymes typically have a recognition site that contains a CpG dinucleotide, and cleavage is blocked if that site is methylated. Sites with many reads are inferred to have low methylation levels, whereas sites with few or no reads are inferred to have high methylation levels. The murine genome contains 1,594,139 CCGG sites, of which 1,130,065 (71%) can be uniquely mapped. Although each restriction enzyme site can generate two library tags, we considered the sum of tag sequences for each restriction enzyme site. A total of 619,060 sites (55%) was located within the promoter and gene body regions of unique genes, and 11% of these were within CpG islands (CGIs). A control library was also constructed by replacing HpaII with MspI, a methylation-insensitive isoschizomer of HpaII. The tags cut with MspI were used for determining zero-tag count or nonhit sites, because no tag from a HpaII library may correspond to a fully methylated site or false negative.

Using the SOLiD platform, ~65 million reads of methylation tags from naive, effector, and memory CD4⁺ T cell genomes cut with HpaII or MspI were aligned to the mouse genome, with at most two mismatches, to allow for sequencing errors and single nucleotide polymorphisms. Thirty-four million (52%) of these tags were aligned to unique sites after repetitive sequences were excluded (Table I). These MSCC data were analyzed for the methylation levels of individual sites based on bisulfite sequencing. When MSCC tag counts and DNA methylation for randomly selected HpaII sites were compared, the number of MSCC methylation tags correlated with the methylation levels derived from bisulfite data, consistent with results reported previously (23) (Fig. 2). Therefore, we defined three categories of methylation sites: low or hypo (median methylation <20%), intermediate (>20 to <80%), and high or hyper (>80%). A total of 65 and 64% of unique CpG sites in naive and memory CD4⁺ T cells, respectively, was hypermethylated, whereas 13% in both naive and memory cells had low methylation. Around TSSs, 28 and 31% of sites in naive and memory cells, respectively, were hypermethylated, whereas 45 and 41%, respectively, had low methylation. In addition, only 28 and 30% of CGIs in naive and memory cells, respectively, were methylated.

Comparison of CpG methylation between naive and memory T cells

To observe changes in DNA methylation during T cell differentiation, the methylation status of CpG sites in gene-associated

FIGURE 3. DMRs in DNA from naive and memory CD4⁺ T cells. DMRs were classified based on their location in promoter (up to 500 bp from a TSS, based on RefSeq annotation), exon, intron, and intergenic regions based on their position relative to known genes. The number of sites represents defined HpaII restriction sites. The p values were calculated using the Fisher exact test.

| No. of DMRs | No. of sites | P -value | Position | No. of DMRs/No. of sites | | | |
|-------------|--------------|------------|-------------------------------|----------------------------------|--------|-------|--------|
| | | | | 0 | 0.0005 | 0.001 | 0.0015 |
| 52 | 96,011 | 3.05E-7 | Promoter+1 st exon | [Bar chart showing distribution] | | | |
| 54 | 84,749 | 2.00E-04 | Exon (2 nd -) | [Bar chart showing distribution] | | | |
| 446 | 438,300 | 9.03E-01 | Intron | [Bar chart showing distribution] | | | |
| 592 | 511,005 | 1.06E-05 | Inter-genic regions | [Bar chart showing distribution] | | | |
| 1144 | 1,130,065 | | Total | [Bar chart showing distribution] | | | |

Table II. Methylation of the 5'-region of naive and memory CD4⁺ T cell genes with a DMR in an intron

| No. of Tags | | No. of Genes (%) |
|-------------------------------|-------------------------------|------------------|
| Naive cells | Memory cells | |
| Hypomethylation (≥ 10) | Hypomethylation (≥ 10) | 273 (87.5) |
| Hypomethylation (≥ 10) | Hypermethylation (≤ 2) | 0 (0) |
| Hypermethylation (≤ 2) | Hypomethylation (≥ 10) | 1 (0.3) |
| Hypermethylation (≤ 2) | Hypermethylation (≤ 2) | 29 (9.3) |
| Obscure methylation | | 9 (2.9) |
| Total | | 312 (100) |

regions (the gene body including 500 bp upstream from the TSS) was compared between naive and memory T cells. When a DMR was defined as a change from 0 to >10 tags at sites cut by MspI, 1144 sites were identified as DMRs during T cell differentiation (Supplemental Table II). Fifty-one percent (552) of these DMRs were in gene-associated regions, and 467 sites associated with 437 genes were unmethylated in memory cells. In contrast, 85 sites associated with 84 genes were methylated in memory cells. The remaining 49% of the DMRs were in intergenic regions. Fig. 3 shows the DMR positions in the genome. The number of DMRs in the 5'-region (500 bp upstream from the TSS and first exon) was significantly lower than in other regions. Many DMRs were located in introns, with a few in CGIs. Our data indicated that DNA methylation in gene-promoter regions did not always correspond to a repressive epigenetic event in CD4⁺ T cells. It is well known that the region upstream of a gene, including the promoter, is

important for gene expression. Thus, we examined the DNA methylation status of gene-upstream regions (promoter and first exon) for DMRs. Others investigators reported a correlation between the methylation status of adjacent CpG sites and a high incidence of short-range comethylation (26, 27). Eighty-eight percent of genes with DMRs showed hypomethylation in their promoter/first exon in naive and memory T cells (Table II). CpG methylation of the first intron and second exon of *Cish* and of the first intron of *Tbx21*, but not of the promoter regions, was different between naive and memory T cells (Fig. 4). The results of MSCC analysis of a series of DMRs was consistent with bisulfite sequencing data. These data suggest that DNA methylation in the gene body (introns and after second exons) may be characteristic of the memory cell phenotype. To identify the function of genes differentially methylated between naive and memory T cells, genes with DMRs were classified using the Gene Ontology Consortium database (GO) (Table III). Genes associated with cell communication, signal transduction, and intracellular signaling pathways tended to be hypomethylated in memory T cells. In contrast, genes associated with development processes and biological regulation tended to be hypomethylated in naive T cells.

DNA methylation and gene expression in memory T cells

To investigate the relationship between gene expression and changes in CpG methylation in DMRs, we analyzed the gene expression of naive cells, in vitro-activated effector cells, and memory CD4⁺ T cells using the Illumina/Solexa sequencing system. More than 12 million 25-base 5'-SAGE tags were obtained from the three libraries and matched to sequences in the

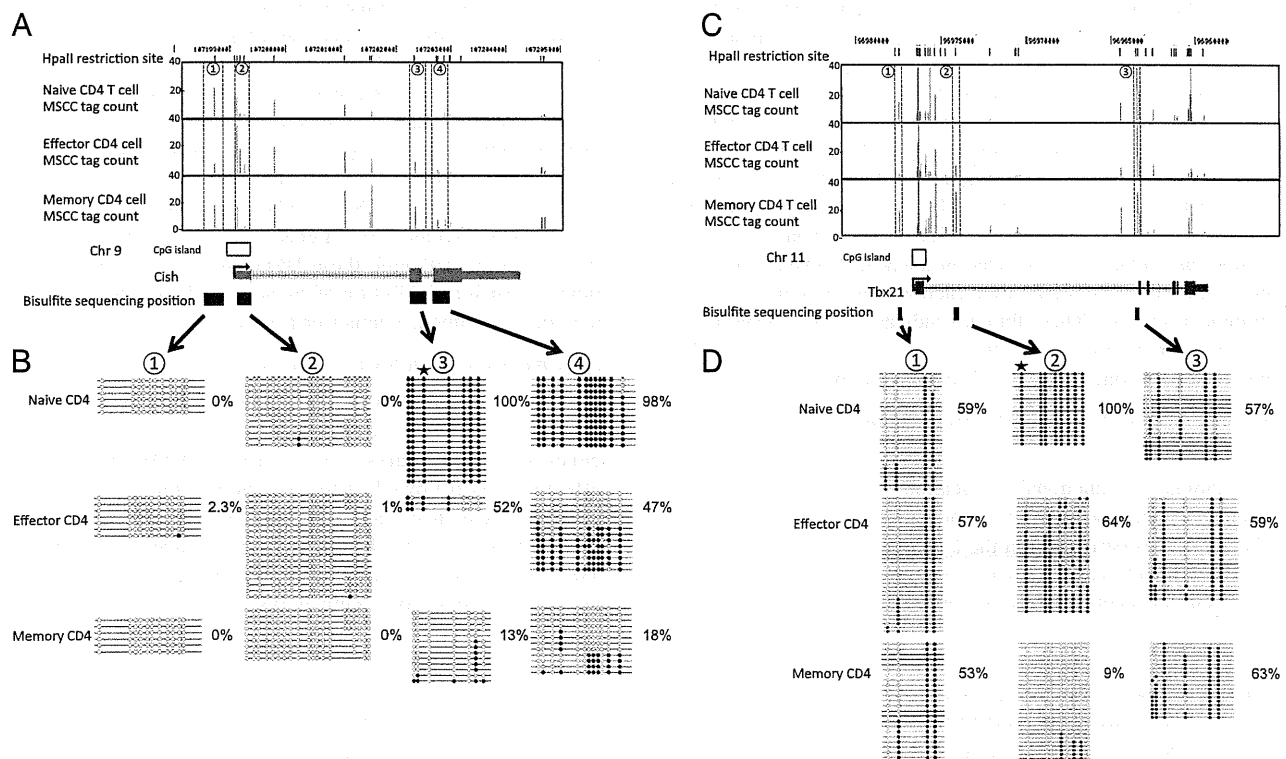


FIGURE 4. DMRs in the *Cish* and *Tbx21* loci of naive, effector, and memory T cells. Genomic organization of the mouse *Cish* (A) and *Tbx21* (C) loci, showing transcription start sites (arrows), single CGI (boxes), and exons (light blue). MSCC analysis of naive, effector, and memory T cells was across the 5'-end of each loci. Each vertical line (brown) represents a mean normalized tag from the MSCC analysis at the genomic location (listed on the x-axis) within the *Cish* and *Tbx21* loci on chromosomes 9 and 11, respectively (University of California, Santa Cruz genome browser). Results of genomic bisulfite sequencing for *Cish* (B) and *Tbx21* (D). Each row of circles represents an individual clone sequenced in the analysis after bisulfite treatment and PCR. Open circles indicate CpG sites at which no DNA methylation was detected. Filled circles indicate CpG sites that were methylated. Stars indicate the position of restriction sites detected by MSCC. Percentage values indicate the DNA methylation ratio of each region, as measured by bisulfite sequencing.

Table III. Gene ontology of DMR-associated genes

| Best GO | Category | Count | Total | <i>p</i> Value ^a |
|----------------------------------|---|-------|-------|-----------------------------|
| Hypomethylated in memory T cells | | | | |
| GO:0007154 | Cell communication | 119 | 5560 | 3.49E-18 |
| GO:0007165 | Signal transduction | 111 | 5142 | 2.65E-17 |
| GO:0007242 | Intracellular signaling pathway | 55 | 1965 | 4.94E-14 |
| GO:0007267 | Cell-cell signaling | 25 | 640 | 5.25E-11 |
| GO:0032502 | Developmental process | 69 | 3347 | 1.20E-08 |
| GO:0007275 | Multicellular organismal development | 53 | 2299 | 1.20E-08 |
| GO:0032501 | Multicellular organismal process | 75 | 3822 | 2.33E-08 |
| GO:0048731 | System development | 39 | 1605 | 5.67E-07 |
| GO:0065007 | Biological regulation | 109 | 6731 | 7.44E-07 |
| GO:0050789 | Regulation of biological process | 101 | 6140 | 1.22E-06 |
| GO:0007215 | Glutamate signaling pathway | 6 | 21 | 3.93E-06 |
| GO:0048519 | Negative regulation of biological process | 30 | 1182 | 7.67E-06 |
| GO:0048856 | Anatomical structure development | 43 | 2005 | 8.94E-06 |
| GO:0009966 | Regulation of signal transduction | 23 | 800 | 8.94E-06 |
| GO:0048523 | Negative regulation of cellular process | 29 | 1137 | 8.96E-06 |
| Hypomethylated in memory T cells | | | | |
| GO:0032502 | Developmental process | 19 | 3347 | 4.57E-06 |
| GO:0065007 | Biological regulation | 29 | 6731 | 4.57E-06 |
| GO:0050789 | Regulation of biological process | 27 | 6140 | 6.68E-06 |
| GO:0016070 | RNA metabolic process | 21 | 4155 | 8.43E-06 |

^aEach category was based on a *p* value < 1.0E-05.

murine genome (Table IV). Seventy-four percent of unique mapped tags were associated with RefSeq cDNA sequences, corresponding to ~12,000–14,000 different protein-coding genes in this cell type (Supplemental Table III). The expression level of 1256 genes was significantly different between naive and effector cells, whereas 259 genes were expressed significantly differently between naive and memory cells (*p* < 0.001, >10-fold difference). The 30 genes with the largest relative difference between effector and naive cells and between memory and naive cells are listed in Table V.

When gene-expression levels and DMRs were compared between naive and memory CD4⁺ T cells, 24 DMRs were associated with increased expression of genes (e.g., CXCR6, Tbx21, Chsy1, and Cish) in memory cells compared with naive cells (>10 tags and >4-fold difference) (Table VI). In contrast, 27 DMRs were associated with decreased expression of other genes (e.g., Maff, Ephb6, and Trpm2). Classification using GO revealed that these genes are related to signal transduction, cell communication, and immune responses. These findings indicate that key genes relating to the memory phenotype undergo variable changes in DNA methylation during CD4⁺ T cell differentiation.

The relationship between DNA methylation and enhancer activity

To examine the functional implications of these DMRs, we constructed a luciferase reporter vector consisting of the EF1 promoter and sequences derived from the DMR in the introns of 15 genes, which positively and negatively correlated with gene expression. Transient transfections were performed in untreated or P/I-treated

EL-4 T cells using unmethylated (CpG) or in vitro SssI-methylated (mCpG) reporter plasmids. The transcriptional activity of the luciferase reporter construct containing the DMR of *Ptgir*, *Tnfrsf4*, *Tbx21*, *Cish*, *Chsy1*, *IL7r*, and *Acot7* genes was 2-fold greater than that of the empty control vector (pCpGL-EF1) (Fig. 5). For these genes, transcriptional activation was reduced following in vitro methylation of the CpGs in the corresponding DMRs, demonstrating a suppressive effect of methylation on enhancer function. In contrast, for the luciferase reporter constructs containing the DMR of seven of the eight genes that showed reduced expression in memory cells compared with naive cells, transcriptional activity was unchanged relative to the empty control vector. Further validation confirmed that MSCC tag counts correlated with bisulfite-sequencing data for these genes. For example, DMRs in *Klf7* and *Mapk1p1* had higher MSCC counts in memory cells (indicating less DNA methylation) but higher expression levels in naive cells (Fig. 6). Thus, although these DMRs may possess an alternative function, such as inhibition of silencer binding to the gene region, they do not influence enhancer activity.

DNA methylation status in T cell subsets

We next investigated DNA methylation in effector CD4⁺ T cells. Effector CD4⁺ T cells were isolated 5 d after Ag stimulation for gene-expression analysis. Interestingly, DMR methylation in effector cells followed different kinetics during differentiation compared with naive and memory cells. DMRs were classified into six distinct groups by DNA-methylation analysis (Table VII). Twenty-seven percent of DMRs were hypermethylated in naive and effector cells but were hypomethylated in memory cells

Table IV. Summary of CD4⁺ T cell sequencing

| Cell Type | Sequenced Tags | Unique Tags | Mapped Tags (one locus) | Tags in RefSeq | Gene No. | Gene No. (>1 copy) |
|-----------------------------------|----------------|-------------|-------------------------|----------------|----------|--------------------|
| CD4 ⁺ naive T cells | 12,088,592 | 7,883,186 | 4,122,853 | 3,382,975 | 14,064 | 8,715 |
| CD4 ⁺ effector T cells | 8,660,468 | 4,547,959 | 4,449,231 | 2,790,122 | 12,877 | 8,756 |
| CD4 ⁺ memory T cells | 11,442,151 | 6,258,543 | 3,916,175 | 3,179,174 | 13,384 | 8,138 |

Unique tags were aligned to a position unambiguously. Unique tags in TSSs were the number of unique tags mapped to regions within 500 bases of the representative TSSs of genes in the RefSeq database. Unique tags were categorized into three groups based on the number of mismatches in individual alignments. Effector T cells were generated from CD4⁺ T cells from DO11.10-Tg mice stimulated with an OVA peptide plus allophycocyanin conditions for 5 d in vitro. Memory CD4⁺ T cells were isolated from spleen and lymph node at 4 wk after cell transfer. 1 copy = 20 tags/3 million tags, because human cells are predicted to contain 300,000 mRNA molecules.

Table V. Gene-expression profile of effector and memory CD4⁺ T cells compared with naive CD4⁺ T cells

| Naive T Cells Effector > Naive | No. of Tags in | | RefSeq | Description |
|-----------------------------------|------------------|----------------|--------------|---|
| | Effector T Cells | Memory T Cells | | |
| 0 | 54,848 | 4 | NM_008630 | Metallothionein 2 |
| 2 | 27,314 | 161 | NM_139198 | Placenta-specific 8 |
| 1 | 2,483 | 7 | NM_011340 | Serine or cysteine proteinase inhibitor clade |
| 0 | 1,837 | 66 | NM_001111099 | Cyclin-dependent kinase inhibitor 1A P21 |
| 1 | 1,620 | 19 | NM_145158 | Elastin microfibril interfacer 2 |
| 0 | 1,354 | 5 | NM_013542 | Granzyme B |
| 1 | 1,100 | 185 | NM_008519 | Leukotriene B4 receptor 1 |
| 5 | 6,117 | 7 | NM_009375 | Thyroglobulin |
| 1 | 931 | 5 | NM_133662 | Immediate early response 3 |
| 1 | 904 | 1 | NM_053095 | IL 24 |
| 0 | 895 | 20 | NM_021397 | Repressor of GATA |
| 2 | 1,461 | 17 | NM_007796 | CTL-associated protein 2 |
| 7 | 5,661 | 3819 | NM_026820 | IFN-induced transmembrane protein 1 |
| 11 | 7,979 | 94 | NM_010370 | Granzyme A |
| 0 | 713 | 4 | NM_001080815 | Gastric inhibitory polypeptide receptor |
| 0 | 543 | 21 | NM_008147 | gp49 A |
| 1 | 448 | 9 | NM_133720 | Cysteinyl leukotriene receptor 2 |
| 2 | 879 | 3 | NM_009150 | Selenium binding protein 1 |
| 50 | 22,626 | 82 | NM_011401 | Solute carrier family 2 facilitated glucose |
| 0 | 453 | 2 | NM_147776 | von Willebrand factor A domain-related protein |
| 3 | 1,202 | 81 | NM_011498 | Basic helix-loop-helix domain containing class |
| 2 | 724 | 0 | NM_008156 | GPI specific |
| 0 | 348 | 1 | NM_178241 | IL-8 receptor α |
| 63 | 21,938 | 26 | NM_013602 | Metallothionein 1 |
| 39 | 13,419 | 53 | NM_001077508 | TNF receptor superfamily |
| 1 | 299 | 38 | NM_008337 | IFN γ |
| 0 | 326 | 4 | NM_001004174 | Hypothetical protein LOC433470 |
| 0 | 325 | 0 | NM_207279 | Phosphatidylinositol-specific phospholipase C X |
| 0 | 322 | 21 | NM_013532 | Leukocyte Ig-like receptor |
| 0 | 319 | 0 | NM_009137 | Chemokine C-C motif ligand 22 |
| Effector < Naive | | | | |
| 1517 | 0 | 159 | NM_009777 | Complement component 1 q subcomponent, B chain |
| 665 | 0 | 93 | NM_007574 | Complement component 1 q subcomponent, C chain |
| 590 | 0 | 39 | NM_007572 | Complement component 1 q subcomponent, A chain |
| 426 | 0 | 43 | NM_001083955 | Hemoglobin α adult chain 2 |
| 407 | 0 | 384 | NM_011703 | Vasoactive intestinal peptide receptor 1 |
| 3535 | 10 | 1,617 | NM_008052 | Deltex 1 homolog |
| 2037 | 7 | 121 | NM_001042605 | CD74 Ag isoform 1 |
| 306 | 0 | 4 | NM_019577 | Chemokine C-C motif ligand 24 |
| 289 | 0 | 14 | NM_007995 | Ficolin A |
| 313 | 1 | 13 | NM_001080934 | Solute carrier family 16 monocarboxylic acid |
| 219 | 0 | 5 | NM_001037859 | Colony stimulating factor 1 receptor |
| 178 | 0 | 139 | NM_033596 | Cistone cluster 2 H4 |
| 146 | 1 | 14 | NM_011414 | Secretory leukocyte peptidase inhibitor |
| 387 | 3 | 302 | NM_013832 | RAS protein activator like 1 GAP1 like |
| 120 | 0 | 19 | NM_133209 | Paired immunoglobulin-like type 2 receptor β |
| 117 | 0 | 9 | NM_008220 | Hemoglobin β adult major chain |
| 96 | 1 | 33 | NM_025806 | Hypothetical protein LOC66857 |
| 78 | 0 | 102 | NM_145227 | 2'-5' oligoadenylate synthetase 2 |
| 78 | 0 | 163 | NM_178185 | Histone cluster 1 H2ao |
| 78 | 0 | 283 | NM_001033813 | Hypothetical protein LOC619310 |
| 85 | 1 | 7 | NM_008076 | γ -aminobutyric acid GABA-C receptor |
| 74 | 0 | 3 | NM_177686 | C-type lectin domain family 12 member a |
| 79 | 1 | 3 | NM_016704 | Complement component 6 |
| 71 | 1 | 6 | NM_009913 | Chemokine C-C motif receptor 9 |
| 64 | 0 | 11 | NM_138673 | Stabilin-2 |
| 64 | 0 | 9 | NM_001024932 | Paired immunoglobulin-like type 2 receptor β 2 |
| 69 | 1 | 5 | NM_011518 | Spleen tyrosine kinase |
| 523 | 9 | 28 | NM_009525 | Wingless-related MMTV integration site 5B |
| 59 | 0 | 4 | NM_009721 | Na ⁺ /K ⁺ -ATPase β 1 subunit |
| 1615 | 28 | 734 | NM_010494 | ICAM 2 |
| Memory > Naive | | | | |
| 7 | 5,661 | 3819 | NM_026820 | IFN-induced transmembrane protein 1 |
| 2 | 13 | 931 | NM_001099217 | Lymphocyte Ag 6 complex locus C2 |
| 15 | 59 | 3884 | NM_010741 | Lymphocyte Ag 6 complex locus C |
| 1 | 1,100 | 185 | NM_008519 | Leukotriene B4 receptor 1 |
| 2 | 122 | 360 | NM_015789 | Dickkopf-like 1 |
| 1 | 5 | 163 | NM_010553 | IL 18 receptor accessory protein |
| 0 | 309 | 179 | NM_031395 | Synaptotagmin-like 3 isoform a |
| 1 | 2 | 146 | NM_009915 | Chemokine C-C motif receptor 2 |

(Table continues)

Table V. (Continued)

| No. of Tags in | | | RefSeq | Description |
|-----------------------------------|------------------|----------------|--------------|---|
| Naive T Cells Effector > Naive | Effector T Cells | Memory T Cells | | |
| 12 | 641 | 1,661 | NM_011313 | S100 calcium binding protein A6 calcyclin |
| 0 | 73 | 129 | NM_177716 | Hypothetical protein LOC239650 |
| 23 | 4,403 | 2,963 | NM_030694 | IFN-induced transmembrane protein 2 |
| 209 | 317 | 22,679 | NM_013653 | Chemokine C-C motif ligand 5 |
| 1 | 114 | 88 | NM_146064 | Acyl-CoA:cholesterol acyltransferase 2 |
| 1 | 3 | 84 | NM_133643 | EDAR ectodysplasin-A receptor-associated death |
| 2 | 27,314 | 161 | NM_139198 | Placenta-specific 8 |
| 3 | 16 | 224 | NM_013599 | Matrix metalloproteinase 9 |
| 1 | 53 | 70 | NM_030712 | Chemokine C-X-C motif receptor 6 |
| 4 | 72 | 268 | NM_011311 | S100 calcium binding protein A4 |
| 3 | 140 | 186 | NM_019507 | T-box 21 |
| 4 | 1,051 | 238 | NM_024253 | NK cell group 7 sequence |
| 0 | 1,837 | 66 | NM_001111099 | Cyclin-dependent kinase inhibitor 1A P21 |
| 1 | 4 | 59 | NM_016685 | Cartilage oligomeric matrix protein |
| 12 | 34 | 815 | NM_009910 | Chemokine C-X-C motif receptor 3 |
| 1 | 0 | 50 | NM_016958 | Keratin 14 |
| 1 | 41 | 44 | NM_008967 | PG I receptor IP |
| 132 | 729 | 5,823 | NM_001013384 | Podocan-like 1 |
| 0 | 31 | 43 | NM_010177 | Fas ligand TNF superfamily member 6 |
| 1 | 299 | 38 | NM_008337 | IFN γ |
| 1 | 1 | 37 | NM_010730 | Annexin A1 |
| 1 | 4 | 36 | NM_018734 | Guanylate nucleotide binding protein 4 |
| Naive > Memory | | | | |
| 817 | 114 | 8 | NM_207231 | ADP-ribosylation-like factor 12 protein |
| 82 | 37 | 1 | NM_175274 | Tweety 3 |
| 306 | 0 | 4 | NM_019577 | Chemokine C-C motif ligand 24 |
| 75 | 74 | 0 | NM_010358 | Gst μ 1 |
| 61 | 52 | 1 | NM_011129 | Septin 4 |
| 53 | 63 | 1 | NM_027406 | Aldehyde dehydrogenase 1 family member 11 |
| 51 | 1 | 1 | NM_029162 | Zinc finger protein 509 |
| 51 | 0 | 1 | NM_008694 | Neutrophilic granule protein |
| 51 | 1 | 1 | NM_153510 | Paired immunoglobulin-like type 2 receptor α |
| 51 | 24 | 1 | NM_007405 | Adenylate cyclase 6 |
| 48 | 37 | 1 | NM_011984 | Homer homolog 3 |
| 148 | 5 | 3 | NM_009238 | SRY-box containing gene 4 |
| 46 | 12 | 1 | NM_013569 | Voltage-gated potassium channel subfamily H, |
| 44 | 10 | 1 | NM_026629 | Hypothetical protein LOC68235 |
| 43 | 25 | 1 | NM_011692 | Von Hippel-Lindau binding protein 1 |
| 219 | 0 | 5 | NM_001037859 | Colony stimulating factor 1 receptor |
| 115 | 22 | 3 | NM_008538 | Myristoylated alanine rich protein kinase C |
| 36 | 22 | 1 | NM_177758 | Zinc finger and SCAN domains 20 |
| 36 | 0 | 1 | NM_013612 | Solute carrier family 11 proton-coupled |
| 36 | 7 | 1 | NM_009223 | Stannin |
| 72 | 18 | 2 | NM_001033929 | Threonine synthase-like 2 |
| 36 | 53 | 0 | NM_011232 | RAD1 homolog |
| 94 | 18 | 3 | NM_011639 | Thyroid receptor-interacting protein 6 |
| 30 | 4 | 1 | NM_133921 | Ovarian zinc finger protein |
| 30 | 110 | 1 | NM_020006 | CDC42 effector protein Rho GTPase binding 4 |
| 33 | 16 | 0 | NM_009372 | TG-interacting factor |
| 29 | 1 | 1 | NM_013667 | Solute carrier family 22 member 2 |
| 28 | 14 | 1 | NM_030557 | Myoneurin |
| 177 | 25 | 6 | NM_001081127 | A disintegrin-like and metalloproteinase |
| 31 | 103 | 0 | NM_033612 | Elastase 1 pancreatic |

The 30 genes with the largest relative differences between effector and naive cells and between memory and naive cells are listed. The total number of tags from naive (3,382,975), effector (2,790,122), and memory (3,179,174) cells was normalized to 3,000,000.

(pattern 1). For example, the extent of DNA methylation in the DMR of *CXCR6* was 92% in naive cells, 80% in effector cells, and 6% in memory T cells (Supplemental Fig. 1). Moreover, 43% of DMRs were hypermethylated in the naive phase, intermediately methylated in the effector phase, and hypomethylated in the memory phase (pattern 2). In *Cish*, for example, DNA methylation in the DMR in the second exon was 100% in naive cells, 52% in effector cells, and 13% in memory cells. An additional 17% of DMRs were hypermethylated in naive cells, intermediately methylated in effector cells, and hypomethylated in memory cells (pattern 3). GO classifications for each DMR methylation pattern revealed that genes in pattern 1 mostly fell into GO categories

related to cell communication and signal transduction, whereas genes in pattern 3 aligned with GO categories related to negative regulation of cellular processes (Table VIII). These data indicate that the timing of methylation changes during T cell differentiation is regulated independently for each gene.

It is well known that central and effector memory T cells are distinct in their differentiation status. Therefore, we also investigated the DNA methylation status of selected DMRs in subpopulations of central and effector memory CD4⁺ T cells from an untreated conventional BALB/c mouse. These DMRs were different across various T cell subsets, reinforcing the finding that the methylation status of T cell subsets reflects T cell differentiation (Fig. 7).

Table VI. Correlation between DNA methylation and gene expression in naive, effector, and memory CD4⁺ T cells

| Restriction Site | Chr | No. of Nucleotides from Nearest TSS | Symbol | Description | RefSeq | Position | Distance from Nearest CGI (bp) | DNA Methylation Score ^a | | | | | | Gene Expression | | | | |
|------------------|-------|-------------------------------------|----------|---|--------------|----------|--------------------------------|------------------------------------|-----------------|---------------------|--------------------|-------------------|------------------|-----------------|------------|-----------|--------------|------------|
| | | | | | | | | Naive Cell HpaII | Naive Cell MspI | Effector Cell HpaII | Effector Cell MspI | Memory Cell HpaII | Memory Cell MspI | N4/M4 Fold | M4/N4 Fold | Naive CD4 | Effector CD4 | Memory CD4 |
| 123716994 | Chr9 | 1,392 | Cxcr6 | Chemokine C-X-C motif receptor 6 | NM_030712 | Intron1 | 43,618 | 0 | 5 | 2 | 7 | 18 | 4 | 0 | 78 | 1 | 53 | 70 |
| 96974152 | Chr11 | 2,440 | Tbx21 | T-box 21 | NM_019507 | Intron1 | -1,727 | 0 | 2 | 8 | 8 | 30 | 5 | 0 | 69 | 3 | 140 | 186 |
| 17493213 | Chr7 | 1,375 | Ptgir | PG I receptor IP | NM_008967 | Intron1 | -876 | 0 | 10 | 5 | 6 | 11 | 6 | 0 | 49 | 1 | 41 | 44 |
| 73291652 | Chr7 | 37,252 | Chsy1 | Carbohydrate chondroitin synthase 1 | NM_001081163 | Intron2 | -37,769 | 0 | 10 | 8 | 9 | 48 | 6 | 0 | 20 | 16 | 127 | 326 |
| 9453075 | Chr15 | 6,536 | Il7r | IL 7 receptor precursor | NM_008372 | Intron2 | 383,054 | 0 | 4 | 6 | 1 | 13 | 5 | 0 | 17 | 29 | 198 | 498 |
| 151561336 | Chr4 | 9,094 | Acot7 | Acyl-CoA thioesterase 7 | NM_133348 | Intron1 | -9,631 | 0 | 5 | 5 | 6 | 12 | 4 | 0 | 14 | 66 | 289 | 949 |
| 107202323 | Chr9 | 3,304 | Cish | Cytokine inducible SH2-containing protein | NM_009895 | Exon_2/3 | -3,446 | 0 | 1 | 8 | 9 | 17 | 5 | 0 | 10 | 53 | 5018 | 528 |
| 107201507 | Chr9 | 2,488 | Cish | Cytokine inducible SH2-containing protein | NM_009895 | Intron1 | -2,630 | 0 | 2 | 0 | 0 | 12 | 1 | 0 | 10 | 53 | 5018 | 528 |
| 112879061 | Chr6 | 17,427 | Srgap3 | SLIT-ROBO Rho GTPase activating protein 3 | NM_080448 | Intron1 | -117,067 | 0 | 16 | 10 | 10 | 20 | 14 | 0 | 9 | 5 | 241 | 46 |
| 41404992 | Chr19 | 54,614 | Pik3ap1 | Phosphoinositide-3-kinase adaptor protein 1 | NM_031376 | Intron3 | -45,447 | 0 | 4 | 4 | 2 | 17 | 4 | 0 | 5 | 5 | 14 | 28 |
| 41404611 | Chr19 | 54,995 | Pik3ap1 | Phosphoinositide-3-kinase adaptor protein 1 | NM_031376 | Intron3 | -45,828 | 0 | 11 | 9 | 15 | 11 | 9 | 0 | 5 | 5 | 14 | 28 |
| 43981837 | Chr4 | 11,264 | Glipr2 | GLI pathogenesis-related 2 | NM_027450 | Intron3 | -11,607 | 0 | 6 | 1 | 2 | 32 | 2 | 0 | 5 | 59 | 795 | 285 |
| 52379040 | Chr2 | 153,059 | Cacnb4 | Calcium channel voltage-dependent, β 4 | NM_001037099 | Intron2 | 99,263 | 0 | 7 | 7 | 10 | 34 | 6 | 0 | 4 | 6 | 3 | 26 |
| 60189952 | Chr2 | 31,367 | Ly75 | Lymphocyte Ag 75 | NM_013825 | Intron11 | -31,177 | 0 | 1 | 4 | 2 | 12 | 5 | 0 | 4 | 12 | 56 | 47 |
| 29371127 | Chr17 | 3,606 | Cpne5 | Copine V | NM_153166 | Intron1 | -3,256 | 0 | 10 | 3 | 11 | 11 | 8 | 0 | 4 | 4 | 37 | 18 |
| 44355013 | Chr17 | 29,493 | Clic5 | Chloride intracellular channel 5 | NM_172621 | Intron1 | -29,555 | 0 | 7 | 10 | 5 | 52 | 9 | 0 | 4 | 4 | 8 | 14 |
| 28393931 | Chr2 | 25,081 | Ralgds | Ral guanine nucleotide dissociation stimulator | NM_009058 | Intron1 | -4,975 | 0 | 8 | 13 | 15 | 10 | 1 | 0 | 4 | 8 | 81 | 32 |
| 155388145 | Chr4 | 342 | Tnfrsf4 | TNF receptor superfamily | NM_011659 | Intron1 | 20,771 | 0 | 5 | 21 | 6 | 22 | 3 | 0 | 4 | 394 | 5522 | 1455 |
| 79745901 | Chr17 | 8,528 | Cdc42ep3 | CDC42 effector protein Rho | NM_026514 | Intron1 | -7,859 | 0 | 9 | 3 | 14 | 15 | 3 | 0 | 4 | 5 | 2 | 19 |
| 27822267 | Chr2 | 80,063 | Col5a1 | GTPase binding 3 Procollagen type V, α 1 | NM_015734 | Intron16 | -80,584 | 0 | 16 | 3 | 9 | 11 | 10 | 0 | 4 | 4 | 1 | 12 |

(Table continues)

Table VI. (Continued)

| Restriction Site | Chr | No. of Nucleotides from Nearest TSS | Symbol | Description | RefSeq | Position | Distance from Nearest CGI (bp) | DNA Methylation Score ^a | | | | | | Gene Expression | | | | |
|------------------|-------|-------------------------------------|---------------|--|--------------|--------------------------|--------------------------------|------------------------------------|-----------------|---------------------|--------------------|-------------------|------------------|-----------------|------------|-----------|--------------|------------|
| | | | | | | | | Naive Cell HpaII | Naive Cell MspI | Effector Cell HpaII | Effector Cell MspI | Memory Cell HpaII | Memory Cell MspI | N4/M4 Fold | M4/N4 Fold | Naive CD4 | Effector CD4 | Memory CD4 |
| 41565822 | Chr6 | 10,256 | Ephb6 | Eph receptor B6 | NM_007680 | Intron6 | -10,660 | 0 | 10 | 7 | 5 | 10 | 11 | 12 | 0 | 207 | 11 | 17 |
| 77375561 | Chr10 | 54,639 | Trpm2 | Transient receptor potential cation channel | NM_138301 | Intron29 | 10,730 | 0 | 5 | 12 | 8 | 10 | 3 | 11 | 0 | 21 | 2 | 2 |
| 58854000 | Chr15 | 59,542 | Mtss1 | Actin monomer-binding protein | NM_144800 | Intron3 | -58,831 | 0 | 4 | 15 | 6 | 21 | 3 | 9 | 0 | 179 | 60 | 19 |
| 79178744 | Chr15 | 637 | Maff | V-maf musculoaponeurotic fibrosarcoma oncogene | NM_010755 | Intron1 | -1,005 | 0 | 2 | 0 | 1 | 16 | 1 | 9 | 0 | 25 | 122 | 3 |
| 38564748 | Chr2 | 5,312 | Nr5a1 | Nuclear receptor subfamily 5 group A, member 1 | NM_139051 | Intron3 | -1,049 | 0 | 9 | 1 | 0 | 10 | 2 | 9 | 0 | 17 | 13 | 2 |
| 75013736 | Chr12 | 4,720 | Hif1a | Hypoxia inducible factor 1 α subunit | NM_010431 | Intron1 | -5,274 | 0 | 10 | 11 | 7 | 21 | 4 | 8 | 0 | 59 | 276 | 8 |
| 49653434 | Chr2 | 10,229 | 2310010M24Rik | Hypothetical protein LOC71897 | NM_027990 | Intron1 | -10,474 | 0 | 7 | 2 | 10 | 13 | 7 | 7 | 0 | 51 | 11 | 8 |
| 124129324 | Chr5 | 4,974 | Clip1 | Restin | NM_019765 | Intron1 | -4,195 | 0 | 1 | 8 | 7 | 10 | 2 | 7 | 0 | 289 | 61 | 44 |
| 124474362 | Chr5 | 7,905 | Vps37b | Vacuolar protein sorting 37B | NM_177876 | Intron1 | -7,571 | 0 | 15 | 0 | 6 | 10 | 10 | 6 | 0 | 2537 | 1085 | 394 |
| 63517774 | Chr14 | 61,260 | Wdfy2 | WD repeat and FYVE domain containing 2 | NM_175546 | Intron2 | -61,692 | 0 | 4 | 35 | 7 | 25 | 2 | 6 | 0 | 30 | 17 | 5 |
| 56872366 | Chr18 | 4,840 | Lmnb1 | Lamin B1 | NM_010721 | Intron1 | -5,420 | 0 | 5 | 1 | 6 | 18 | 2 | 6 | 0 | 73 | 53 | 12 |
| 3378068 | Chr10 | 179,872 | Oprm1 | Opioid receptor μ 1 | NM_001039652 | Intron3 | 243,866 | 0 | 7 | 3 | 14 | 14 | 6 | 5 | 0 | 30 | 3 | 6 |
| 5574804 | Chr10 | 159,689 | Esr1 | Estrogen receptor 1 α | NM_007956 | Intron3 | -58,813 | 0 | 16 | 1 | 9 | 11 | 13 | 5 | 0 | 46 | 7 | 9 |
| 66089658 | Chr17 | 32,361 | Rab31 | Rab31-like | NM_133685 | Intron1 | -31,962 | 0 | 3 | 5 | 4 | 23 | 5 | 5 | 0 | 19 | 27 | 4 |
| 54300515 | Chr13 | 13,018 | Hrh2 | Histamine receptor H 2 isoform 1 | NM_001010973 | Intron1 | -13,119 | 0 | 6 | 1 | 10 | 14 | 0 | 5 | 0 | 32 | 4 | 7 |
| 71926521 | Chr12 | 21 | Frdm6 | FERM domain containing 6 | NM_028127 | Exon_1/ 14_first exon | 0 | 0 | 4 | 8 | 0 | 14 | 1 | 4 | 0 | 38 | 31 | 9 |
| 58574849 | Chr6 | 28,184 | Abcg2 | ATP-binding cassette subfamily G, member 2 | NM_011920 | Intron1 | 15,477 | 0 | 6 | 7 | 1 | 10 | 0 | 4 | 0 | 39 | 103 | 9 |
| 88790629 | Chr12 | 5,768 | 1810035L17Rik | Hypothetical protein LOC380773 | NM_026958 | Intron3 | -6,286 | 0 | 4 | 6 | 2 | 15 | 9 | 4 | 0 | 34 | 130 | 9 |
| 64135805 | Chr1 | 32,156 | Klf7 | Kruppel-like factor 7 ubiquitous | NM_033563 | Intron1 | -32,381 | 0 | 6 | 4 | 11 | 17 | 1 | 4 | 0 | 108 | 48 | 27 |
| 21359913 | Chr2 | 70,720 | Gpr158 | G protein-coupled receptor 158 | NM_001004761 | Intron2 | -69,515 | 0 | 8 | 0 | 3 | 13 | 10 | 4 | 0 | 11 | 3 | 3 |
| 13609664 | Chr8 | 67,921 | Rasa3 | RAS p21 protein activator 3 | NM_009025 | intron3 | -67,326 | 0 | 8 | 5 | 2 | 14 | 6 | 4 | 0 | 570 | 349 | 157 |
| 24828918 | Chr8 | 48,754 | Zmat4 | Zinc finger matrin type 4 | NM_177086 | intron1 | -48,830 | 0 | 10 | 3 | 14 | 11 | 16 | 4 | 0 | 40 | 5 | 11 |

(Table continues)

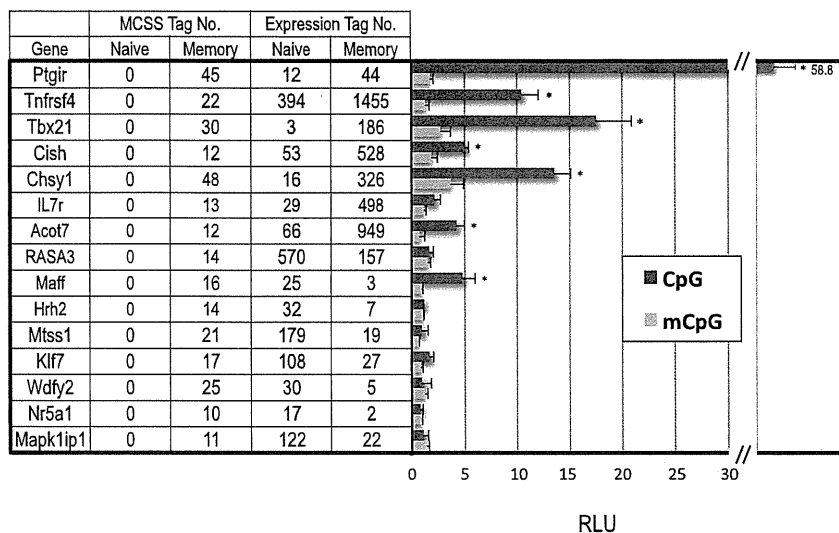
Table VI. (Continued)

| Restriction Site | Chr | No. of Nucleotides from Nearest TSS | Symbol | Description | RefSeq | Position | Distance from Nearest CGI (bp) | DNA Methylation Score ^a | | | | | | Gene Expression | | | | |
|------------------|-------|-------------------------------------|----------|---|--------------|-----------------------|--------------------------------|------------------------------------|-----------------|---------------------|--------------------|-------------------|------------------|-----------------|------------|-----------|--------------|------------|
| | | | | | | | | Naive Cell HpaII | Naive Cell MspI | Effector Cell HpaII | Effector Cell MspI | Memory Cell HpaII | Memory Cell MspI | N4/M4 Fold | M4/N4 Fold | Naive CD4 | Effector CD4 | Memory CD4 |
| 146036806 | Chr7 | 1,142 | Mapk1ip1 | MAPK-interacting and spindle-stabilizing T-box 21 | NM_001045483 | intron1 | -827 | 0 | 7 | 3 | 5 | 11 | 5 | 4 | 0 | 233 | 152 | 66 |
| 96960335 | Chr11 | 16,257 | Tbx21 | | NM_019507 | Exon_6/ 6_lastExon | -15,544 | 19 | 1 | 1 | 0 | 0 | 2 | 0 | 69 | 3 | 140 | 186 |
| 94729332 | Chr1 | 1,070 | Gpc1 | Glypican 1 | NM_016696 | Intron1 | 0 | 16 | 2 | 0 | 0 | 0 | 1 | 0 | 21 | 11 | 22 | 227 |
| 128915487 | Chr4 | 10,198 | C77080 | Hypothetical protein LOC97130 | NM_001033189 | Intron1 | -581 | 12 | 3 | 1 | 1 | 0 | 2 | 0 | 6 | 3 | 3 | 15 |
| 148238956 | Chr4 | 60,456 | Casz1 | Castor homolog 1 zinc finger | NM_027195 | Intron2 | 26,131 | 10 | 17 | 1 | 16 | 0 | 7 | 0 | 4 | 10 | 13 | 36 |
| 120328900 | Chr2 | 39,292 | Capn3 | Calpain 3 isoform a | NM_007601 | Exon_21/24 | 60,309 | 15 | 7 | 2 | 6 | 0 | 13 | 22 | 0 | 61 | 9 | 3 |
| 35990963 | Chr18 | 1,492 | Cxxc5 | CXXC finger 5 | NM_133687 | Intron1 | 0 | 28 | 4 | 9 | 2 | 0 | 1 | 13 | 0 | 12 | 22 | 1 |
| 126838794 | Chr8 | 83,501 | Galnt2 | UDP-N-acetyl- α -D-galactosamine: polypeptide WD repeat and FYVE domain containing 2 | NM_139272 | Intron3 | -83,718 | 16 | 5 | 0 | 2 | 0 | 1 | 8 | 0 | 128 | 55 | 16 |
| 63546881 | Chr14 | 90,367 | Wdfy2 | | NM_175546 | Intron4 | -90,799 | 20 | 1 | 1 | 9 | 0 | 6 | 6 | 0 | 30 | 17 | 5 |

The category was represented using the criteria of DMRs (changing from 0 to >10 tags at the sites able to be digested by MspI between naive and memory CD4 T cells) and gene expression (memory or naive; >10 tags and >4-fold difference). Each number of gene-expression tags from naive (3,382,975), effector (2,790,122), and memory (3,179,174) cells was normalized to 3,000,000.

^aDNA methylation score is described in *Materials and Methods*.

FIGURE 5. Transcriptional activity of a luciferase reporter gene in unmethylated and methylated DMR sequences from the introns of 15 genes. Transient transfections were performed with a control plasmid (pCpGL-EF1 promoter) or pCpGL-EF-DMR in P/I-treated EL-4 T cells using unmethylated (CpG) or in vitro SssI methylated (mCpG) reporter plasmids. Firefly raw light unit (RLU) data were normalized to *Renilla* luciferase activity relative to the control vector with no insert. * $p < 0.05$, unmethylated versus methylated plasmids, paired Student *t* test.



Discussion

Following activation with Ag, naive T cells differentiate into short-lived effector T cells and long-lived memory T cells. However, the molecular mechanisms behind the generation and maintenance of memory CD4⁺ T cells remain unclear. To address this problem, we studied changes in epigenetic modification and gene expression in Ag-specific CD4⁺ T cells using massive parallel DNA sequencing.

Phenotypically, both naive and memory T cell subsets are made up of small resting cells with upregulated IL-7R expression, which is necessary for their survival in vivo. Effector and memory T cells exhibit increased expression of adhesion markers (e.g., CD44 and LFA-1) and decreased expression of the lymph node homing receptor CD62L (28). This expression pattern was confirmed in the current study. Furthermore, our analyses indicated that, compared with naive CD4⁺ T cells, the genes that were upregulated in memory CD4⁺ T cells (e.g., IL-7R, Bcl2, Bcl2l1, and Cdkn1a and the chemokine-related genes CCL5, CCR2, CXCR6, and CXCR3) were related to cytokine production and development and maintenance of the memory phase. Expression of the Th1 genes IFN- γ , Tbx21, and IL18RAP also increased in memory CD4⁺ T cells. In

addition, the expression of several other genes [i.e., IFN-induced trans-membrane protein 1 (IFITM1) (29), Dkk1 (30), and Il18rap (31)], which are related to proliferative capacity and Th1-type immunological reactions, increased in memory CD4⁺ T cells compared with naive T cells.

It is well known that gene expression involves activation of transcription factors and/or epigenetic changes in the genome. CpG dinucleotides upstream of genes that are active in a particular tissue or cell type are less methylated, whereas inactive genes are surrounded by highly condensed chromatin and have densely methylated upstream CpG dinucleotides. A useful technique for gauging gene accessibility in the chromatin context is to monitor sensitivity of the relevant DNA sequences to digestion with DNase I in intact nuclei (32). In general, genome sites encoding genes located in active chromatin that are actively transcribed or that have the potential to be transcribed upon stimulation are more sensitive to DNase I digestion than are sites encoding genes in inactive or closed chromatin. In this study, we used the recently developed MSCC method that enables cost-effective, high-throughput, genome-wide identification of methylated CpG sites. We identi-

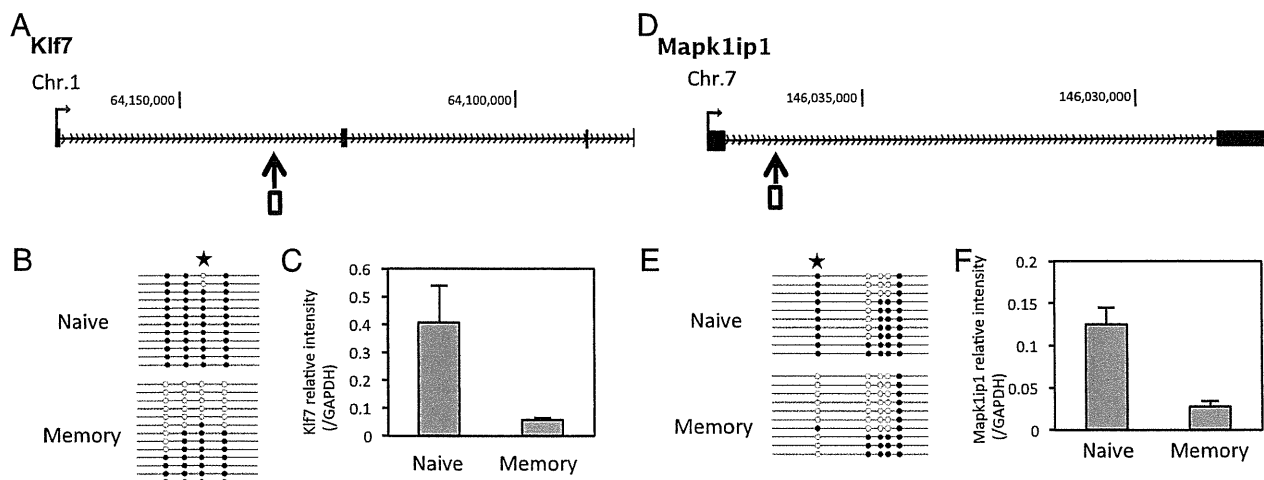


FIGURE 6. DMRs in the *Mapk1p1* and *Klf7* loci of naive and memory T cells. Genomic organization of the mouse *Klf7* (A) and *Mapk1p1* (D) loci showing transcription start sites (\rightarrow), exons (black boxes), DMRs that were detected by MSCC (\uparrow), and bisulfite sequencing positions (white boxes). (B and E) Results of genomic bisulfite sequencing, where each row of circles represents an individual clone sequenced following bisulfite treatment and PCR. Open circles indicate CpG sites at which no DNA methylation was detected. Stars indicate the position of restriction sites detected by MSCC. Filled circles indicate CpG sites that were methylated. (C and F) Downregulated gene expression in memory CD4 T cells measured by quantitative real-time PCR. RT-PCR was performed as described in *Materials and Methods*.

Table VII. DNA methylation status of DMRs in naive, effector, and memory CD4⁺ T cells

| Pattern | DNA Methylation Status | | | No. of DMR (%) |
|---------|------------------------|----------|--------|----------------|
| | Naive | Effector | Memory | |
| 1 | High | High | Low | 314 (27%) |
| 2 | High | Int | Low | 495 (43%) |
| 3 | High | Low | Low | 198 (17%) |
| 4 | Low | Low | High | 25 (2%) |
| 5 | Low | Int | High | 42 (4%) |
| 6 | Low | High | High | 70 (6%) |
| | Total | | | 1144 (100%) |

High, High methylation status (≤ 2); Int, intermediate methylation status (3–9 tags); Low, low methylation status (> 9 tags).

fied 1,144 regions in the mouse genome that were differentially methylated in the process of T cell differentiation. All of these DMRs were in gene body sites without CGIs, highlighting the fact that DNA methylation can occur at sites other than CGIs. Irizarry et al. (33) reported that methylation of CGI shores that exist in close proximity (~ 2 kb) to CGIs is closely associated with tran-

scriptional inactivation. Most tissue-specific DNA methylation seems not to occur within CGI, but rather at CGI shores. However, our data demonstrate that most DMRs in naive and memory CD4⁺ T cells are not associated with CGI or CGI shores. Furthermore, most DMRs in naive and memory CD4⁺ T cells were located in gene bodies, rather than in the promoter regions, as is the case for tumor cells.

Of the DMRs identified in naive and memory CD4⁺ T cells, 51 were potentially associated with gene expression. Gene body methylation is common in ubiquitously expressed genes and is correlated with gene expression (23). Furthermore, intergenic methylation recently was reported to play a major role in regulating cell context-specific alternative promoters in gene bodies (34). In contrast, several groups (19, 35, 36) reported that, in human and mouse regulatory T cells, the majority of DMRs are located at promoter-distal sites and that many of these regions display DNA methylation-dependent enhancer activity in reporter gene assays. Tsuji-Takayama et al. (37) demonstrated that production of IL-10 in regulatory T cells was enhanced by IL-2 through a STAT5-responsive intron enhancer in the IL-10 locus. However, Lai et al. (38) reported that DNA methylation in an

Table VIII. GOs classified by methylation state of DMRs in effector cells

| GO | Genes | Count | Total | <i>p</i> Value |
|---------------------------|---|-------|-------|----------------|
| Hyper(N)-Hyper(E)-Hypo(M) | | | | |
| GO:0007154 | Cell communication | 25 | 5560 | 0.00507 |
| GO:0007165 | Signal transduction | 23 | 5142 | 0.00772 |
| GO:0016477 | Cell migration | 5 | 233 | 0.00772 |
| GO:0006928 | Cell motility | 6 | 383 | 0.00772 |
| GO:0051674 | Localization of cell | 6 | 383 | 0.00772 |
| GO:0022610 | Biological adhesion | 9 | 960 | 0.00772 |
| GO:0007155 | Cell adhesion | 9 | 960 | 0.00772 |
| Hyper(N)-Int(E)-Hypo(M) | | | | |
| GO:0007154 | Cell communication | 74 | 5560 | 6.09E-12 |
| GO:0007165 | Signal transduction | 69 | 5142 | 2.71E-10 |
| GO:0007242 | Intracellular signal transduction | 33 | 1965 | 2.85E-07 |
| GO:0007275 | Multicellular organismal development | 33 | 2299 | 6.72E-05 |
| GO:0007267 | Cell-cell signaling | 17 | 640 | 8.05E-05 |
| GO:0032502 | Developmental process | 42 | 3347 | 0.000126 |
| GO:0051179 | Localization | 51 | 4481 | 0.000243 |
| GO:0007215 | Glutamate signaling pathway | 4 | 21 | 0.00075 |
| GO:0032501 | Multicellular organismal process | 44 | 3822 | 0.000793 |
| GO:0009966 | Regulation of signal transduction | 17 | 800 | 0.000793 |
| GO:0048731 | System development | 23 | 1605 | 0.00236 |
| GO:0051234 | Establishment localization | 45 | 4135 | 0.00298 |
| GO:0006810 | Transport | 44 | 4035 | 0.00327 |
| GO:0050789 | Regulation of biological process | 60 | 6140 | 0.00428 |
| GO:0007268 | Synaptic transmission | 9 | 290 | 0.00434 |
| GO:0048856 | Anatomical structure development | 26 | 2005 | 0.00472 |
| GO:0065007 | Biological regulation | 64 | 6731 | 0.00472 |
| Hyper(N)-Hypo(E)-Hypo(M) | | | | |
| GO:0048523 | Negative regulation of cellular process | 13 | 1137 | 0.000127 |
| GO:0048519 | Negative regulation of biological process | 13 | 1182 | 0.000127 |
| GO:0050794 | Regulation of cellular process | 26 | 5704 | 0.000748 |
| GO:0065007 | Biological regulation | 28 | 6731 | 0.00227 |
| GO:0050789 | Regulation of biological process | 26 | 6140 | 0.00289 |
| GO:0018212 | Peptidyl-tyrosine modification | 3 | 44 | 0.0064 |
| GO:0007242 | Intracellular signal transduction | 13 | 1965 | 0.0072 |
| GO:0007165 | Signal transduction | 22 | 5142 | 0.00765 |
| GO:0007154 | Cell communication | 23 | 5560 | 0.00893 |
| Hypo(N)-Int(E)-Hyper(M) | | | | |
| GO:0007275 | Multicellular organismal development | 9 | 2299 | 0.00989 |
| GO:0032501 | Multicellular organismal process | 11 | 3822 | 0.00989 |
| Hypo(N)-Hypo(E)-Hyper(M) | | | | |
| None | | | | |
| Hypo(N)-Hyper(E)-Hyper(M) | | | | |
| None | | | | |

GOs with a *p* value < 0.01 are shown.

E, Effector T cells; Hyper, hypermethylation status (more than nine tags); Hypo, hypomethylation status (two or fewer tags); Int, intermediate methylation status (three to nine tags); M, memory T cells; N, naive T cells.

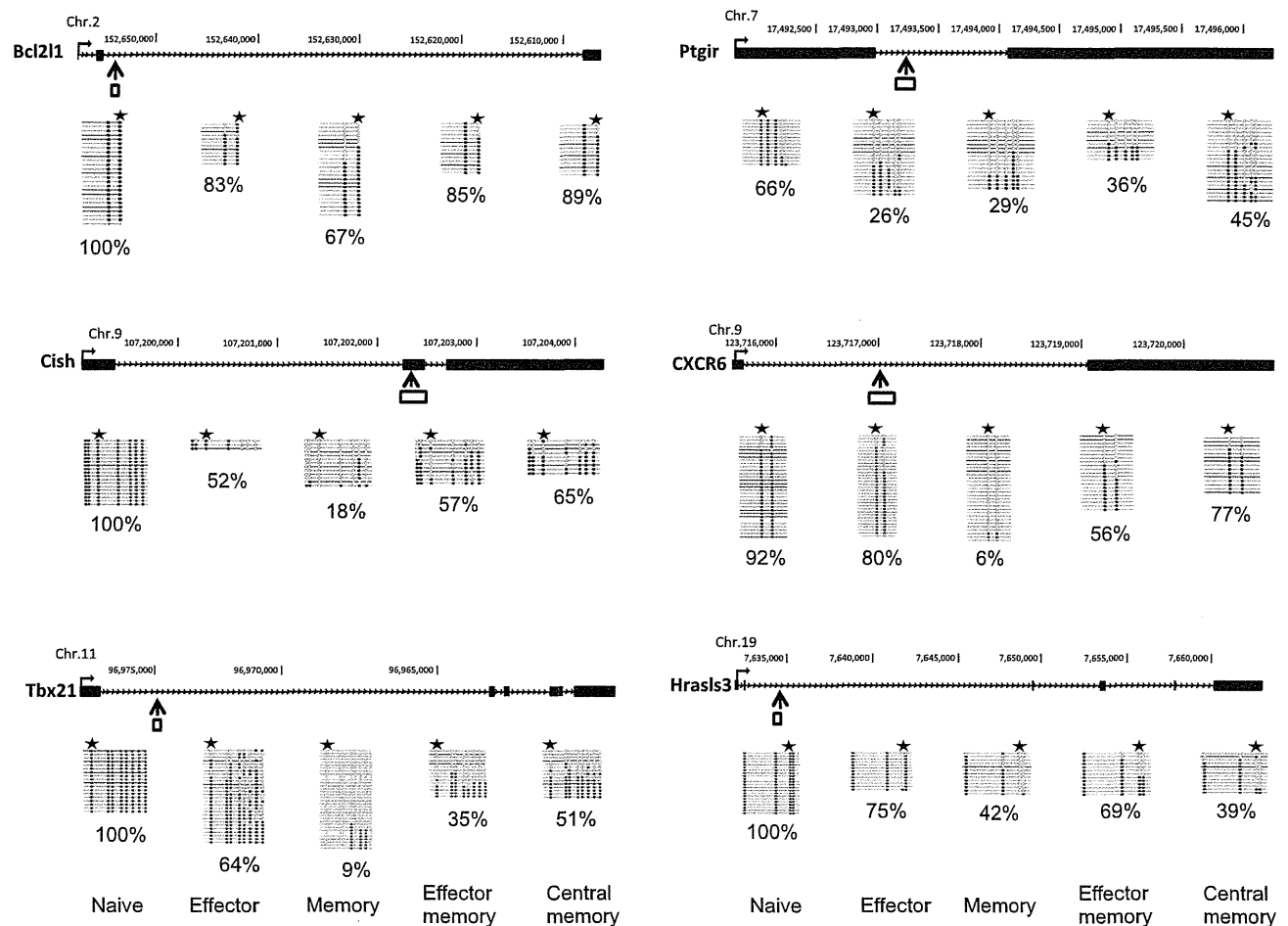


FIGURE 7. DNA methylation status of selected DMRs in subpopulations of central and effector memory $CD4^+$ T cells. $CD62L^+ CCR7^+$ and $CD62L^- CCR7^- CD4^+$ T cells from BALB/c mice were isolated to represent “central memory” and “effector memory” T cells, respectively. Genomic organization of the mouse *Cish*, *Hras3l3*, *Tbx21*, *CXCR6*, *Bcl2l1*, and *Ptgir* loci, showing transcription start sites (\rightarrow), exons (black box), DMRs that were detected by MSCC (\uparrow), and bisulfite sequencing position (white box). Graphs show results of genomic bisulfite sequencing, where each row of circles represents an individual clone sequenced in the analysis after bisulfite treatment and PCR. Open circles indicate CpG sites at which no DNA methylation was detected. Filled circles indicate CpG sites that were methylated. Stars indicate the position of restriction sites detected by MSCC. Percentage values indicate the DNA methylation ratio of each region, as measured by bisulfite sequencing.

intron can prevent enhancer-blocking transcription factor-mediated silencing. We used a reporter assay to examine the 51 gene-expression-associated DMRs and obtained results consistent with earlier reports. When loci containing DMRs were cloned into the reporter gene plasmid, the DMRs possessed enhancer activity in naive T cells in which DNA methylation was suppressed. Like previous studies, our results revealed different enhancer activities for different DMRs. It was reported that, compared with normal control cells, the DNA methylation of gene promoter regions differed in $CD4^+$ T cells in patients with rheumatoid arthritis (39), subacute cutaneous lupus erythematosus (40), and systemic lupus erythematosus (41). Together, these results suggest that, in the normal immune state, these DMRs are associated with enhancer activity rather than with promoter activity.

Genes associated with the 51 gene-expression-associated DMRs in naive and memory $CD4^+$ T cells were functionally categorized as relating to signal transduction, cell communication, and immune responses. As predicted, *IL-7R*, *Bcl2l1*, *Tbx21*, and *CXCR6* genes were associated with changes in DNA methylation. Kim et al. (42) reported that DNA methylation is involved in regulating *IL-7R* expression in T cells. They found that *IL-7R α* high $CD8^+$ T cells had stronger cell signaling and survival responses to *IL-7* compared with *IL-7R α* low $CD8^+$ T cells. Together with these findings, our

results indicate that DNA methylation of the *IL-7R* gene in $CD4^+$ T cells may be a key mechanism for modifying *IL-7*-mediated T cell development and survival. In addition, in the current study, expression of *Tbx21*, as well as of the Th1-related gene *Ptgir*, was also correlated with DNA methylation. Lymph node cells from sensitized *Ptgir*^{-/-} mice show reduced IFN- γ production and a smaller T-bet⁺ subset compared with control mice (43).

There were also several genes relating to memory $CD4^+$ T cells homing to bone marrow (BM) that were associated with changes in DNA methylation. Tokoyada et al. (44) reported that >80% of *Ly-6C^{hi}CD44^{hi}CD62L⁻* memory $CD4^+$ T lymphocytes reside in the BM of adult mice and associate with *IL-7*-expressing VCAM-1 stroma cells. Our results demonstrate that *Ly-6C* is expressed more highly in memory $CD4^+$ T cells than in naive $CD4^+$ T cells. Because *IL-7* is the main cytokine required for $CD4^+$ T cell survival (45), the BM is predicted to function as a survival niche for memory $CD4^+$ T cells. Thus, in the memory phase of immunity, memory Th cells are maintained in BM as resting, but highly reactive, cells in niches defined by *IL-7*-expressing stroma cells. In addition, when gene expression between *CD44^{hi}CD62L⁻CD4⁺* T cells from the spleen and BM were compared, *CD24*, *CD122*, *CXCR6*, and *CCR2* levels on *CD44^{hi}CD62L⁻CD4⁺* T cells from the BM were higher than on the same cells from the spleen (45).

Our data also reveal upregulation of gene expression and unmethylation of *CXCR6* in the memory phase, suggesting that the unmethylation of DNA in gene body regions may be related to the homing of CD44^{hi}CD62L⁻CD4⁺ T cells to the BM.

In memory CD4⁺ T cells, the genes *Chsy1* and *Itgb1* were linked to changes in DNA methylation in introns. *Chsy1* synthesizes chondroitin sulfate and regulates many biological processes, including cell proliferation, recognition, and extracellular matrix deposition. Yin (46) showed that *Chsy1* is the most prominent secreted protein in myeloma cell–osteoclast coculture conditioned medium and that *Chsy1* activates Notch2 signaling in myeloma cells in the BM microenvironment. Therefore, *Chsy1* may play an important role in cell–cell interactions, such as those between T cells and osteoclasts in the BM microenvironment. In contrast, *Itgb1* is critical for maintenance of Ag-specific CD4⁺ T cells in the BM (47). Therefore, DNA methylation in gene body regions is likely to play an important role in CD4⁺ T cell homing to BM.

The expression of *Cish* was also associated with changes in DNA methylation in gene body regions. *Cish* is a member of the SOCS family, which was discovered as a negative regulator of cytokine signaling. However, in CD4 promoter-driven *Cish*-Tg mice, elevated *Cish* expression promotes T cell proliferation and survival after TCR activation relative to T cells in control mice (48). Moreover, Nakajima et al. (49) showed that expression of both *Cish* mRNA and protein is significantly increased in allergen-stimulated CD4⁺ T cells from hen egg–allergic patients relative to patients not allergic to hen eggs. In addition, Khor et al. (50) identified a panel of *Cish* single nucleotide polymorphisms associated with increased susceptibility to infectious diseases, such as bacteremia, malaria, and tuberculosis. Thus, *Cish* expression caused by demethylation within the *Cish* locus in memory T cells may play a role in some infectious and allergic diseases.

In the current study, differences in methylated regions between naive and memory CD4⁺ T cells did not always correlate with gene expression. The promoter and enhancer regions of differentially expressed genes were unmethylated, even in naive CD4⁺ T cells. Therefore, gene expression in the naive phase is likely to be regulated primarily by the activation of transcription factors. However, changes in the DNA methylation of unsynchronized genes may prepare T cells for rapid responses following secondary stimulation via TCR signaling or other stimuli, such as inflammatory cytokines, bacteria, and viruses.

Variable DNA methylation of the enhancers of genes related to T cell development and survival represents a novel mechanism underlying the regulation of gene expression in memory CD4⁺ T cells. In this study, we demonstrated the important role that methylation and demethylation of DNA in exons and introns play in regulating gene-expression patterns in Ag-specific memory CD4⁺ T cells.

Acknowledgments

We thank Dr. Yong-Jun Lee and Ryu Takahashi for technical assistance and Dr. M. Klug (Department of Hematology and Oncology, University Hospital, Regensburg, Germany), for the plasmid pCpG-basic.

Disclosures

The authors have no financial conflicts of interest.

References

- Seder, R. A., and R. Ahmed. 2003. Similarities and differences in CD4⁺ and CD8⁺ effector and memory T cell generation. *Nat. Immunol.* 4: 835–842.
- Moulton, V. R., and D. L. Farber. 2006. Committed to memory: lineage choices for activated T cells. *Trends Immunol.* 27: 261–267.
- Sawalha, A. H. 2008. Epigenetics and T-cell immunity. *Autoimmunity* 41: 245–252.
- Wilson, C. B., E. Rowell, and M. Sekimata. 2009. Epigenetic control of T-helper-cell differentiation. *Nat. Rev. Immunol.* 9: 91–105.
- Cuddapah, S., A. Barski, and K. Zhao. 2010. Epigenomics of T cell activation, differentiation, and memory. *Curr. Opin. Immunol.* 22: 341–347.
- Portela, A., and M. Esteller. 2010. Epigenetic modifications and human disease. *Nat. Biotechnol.* 28: 1057–1068.
- Jaenisch, R., and A. Bird. 2003. Epigenetic regulation of gene expression: how the genome integrates intrinsic and environmental signals. *Nat. Genet.* 33 (Suppl.): 245–254.
- Bird, A. 2002. DNA methylation patterns and epigenetic memory. *Genes Dev.* 16: 6–21.
- Jones, P. A., and D. Takai. 2001. The role of DNA methylation in mammalian epigenetics. *Science* 293: 1068–1070.
- Li, E. 2002. Chromatin modification and epigenetic reprogramming in mammalian development. *Nat. Rev. Genet.* 3: 662–673.
- Meehan, R. R. 2003. DNA methylation in animal development. *Semin. Cell Dev. Biol.* 14: 53–65.
- Lee, P. P., D. R. Fitzpatrick, C. Beard, H. K. Jessup, S. Lehar, K. W. Makar, M. Pérez-Melgosa, M. T. Sweetser, M. S. Schlissel, S. Nguyen, et al. 2001. A critical role for Dnmt1 and DNA methylation in T cell development, function, and survival. *Immunity* 15: 763–774.
- Carbone, A. M., P. Marrack, and J. W. Kappler. 1988. Demethylated CD8 gene in CD4⁺ T cells suggests that CD4⁺ cells develop from CD8⁺ precursors. *Science* 242: 1174–1176.
- Wilson, C. B., K. W. Makar, and M. Pérez-Melgosa. 2002. Epigenetic regulation of T cell fate and function. *J. Infect. Dis.* 185(Suppl. 1): S37–S45.
- Schwab, J., and H. Illges. 2001. Regulation of CD21 expression by DNA methylation and histone deacetylation. *Int. Immunol.* 13: 705–710.
- Chen, S. C., C. Y. Lin, Y. H. Chen, H. Y. Fang, C. Y. Cheng, C. W. Chang, R. A. Chen, H. L. Tai, C. H. Lee, M. C. Chou, et al. 2006. Aberrant promoter methylation of EDNRB in lung cancer in Taiwan. *Oncol. Rep.* 15: 167–172.
- Makar, K. W., and C. B. Wilson. 2004. DNA methylation is a nonredundant repressor of the Th2 effector program. *J. Immunol.* 173: 4402–4406.
- Lindahl Allen, M., C. M. Koch, G. K. Clelland, I. Dunham, and M. Antoniou. 2009. DNA methylation-histone modification relationships across the desmin locus in human primary cells. *BMC Mol. Biol.* 10: 51.
- Schmidl, C., M. Klug, T. J. Boeld, R. Andreesen, P. Hoffmann, M. Edinger, and M. Rehli. 2009. Lineage-specific DNA methylation in T cells correlates with histone methylation and enhancer activity. *Genome Res.* 19: 1165–1174.
- Chappell, C., C. Beard, J. Altman, R. Jaenisch, and J. Jacob. 2006. DNA methylation by DNA methyltransferase 1 is critical for effector CD8 T cell expansion. *J. Immunol.* 176: 4562–4572.
- Kersh, E. N. 2006. Impaired memory CD8 T cell development in the absence of methyl-CpG-binding domain protein 2. *J. Immunol.* 177: 3821–3826.
- Yamashita, M., R. Shinnakasu, Y. Nigo, M. Kimura, A. Hasegawa, M. Taniguchi, and T. Nakayama. 2004. Interleukin (IL)-4-independent maintenance of histone modification of the IL-4 gene loci in memory Th2 cells. *J. Biol. Chem.* 279: 39454–39464.
- Ball, M. P., J. B. Li, Y. Gao, J. H. Lee, E. M. LeProust, I. H. Park, B. Xie, G. Q. Daley, and G. M. Church. 2009. Targeted and genome-scale strategies reveal gene-body methylation signatures in human cells. *Nat. Biotechnol.* 27: 361–368.
- Hashimoto, S., W. Qu, B. Ahsan, K. Ogoshi, A. Sasaki, Y. Nakatani, Y. Lee, M. Ogawa, A. Ametani, Y. Suzuki, et al. 2009. High-resolution analysis of the 5'-end transcriptome using a next generation DNA sequencer. *PLoS ONE* 4: e4108.
- Beissbarth, T., and T. P. Speed. 2004. GOSTat: find statistically overrepresented Gene Ontologies within a group of genes. *Bioinformatics* 20: 1464–1465.
- Eckhardt, F., J. Lewin, R. Cortese, V. K. Rakan, J. Attwood, M. Burger, J. Burton, T. V. Cox, R. Davies, T. A. Down, et al. 2006. DNA methylation profiling of human chromosomes 6, 20 and 22. *Nat. Genet.* 38: 1378–1385.
- Irizarry, R. A., C. Ladd-Acosta, B. Carvalho, H. Wu, S. A. Brandenburg, J. A. Jeddelloh, B. Wen, and A. P. Feinberg. 2008. Comprehensive high-throughput arrays for relative methylation (CHARM). *Genome Res.* 18: 780–790.
- Moulton, V. R., N. D. Bushar, D. B. Leiser, D. S. Patke, and D. L. Farber. 2006. Divergent generation of heterogeneous memory CD4 T cells. *J. Immunol.* 177: 869–876.
- Yang, G., Y. Xu, X. Chen, and G. Hu. 2007. IFITM1 plays an essential role in the antiproliferative action of interferon-gamma. *Oncogene* 26: 594–603.
- Gattinoni, L., X. S. Zhong, D. C. Palmer, Y. Ji, C. S. Hinrichs, Z. Yu, C. Wrzesinski, A. Boni, L. Cassard, L. M. Garvin, et al. 2009. Wnt signaling arrests effector T cell differentiation and generates CD8⁺ memory stem cells. *Nat. Med.* 15: 808–813.
- Debets, R., J. C. Timans, T. Churakowa, S. Zurawski, R. de Waal Malefyt, K. W. Moore, J. S. Abrams, A. O'Garra, J. F. Bazan, and R. A. Kastelein. 2000. IL-18 receptors, their role in ligand binding and function: anti-IL-18R α antibody, a potent antagonist of IL-18. *J. Immunol.* 165: 4950–4956.
- Rao, A., and O. Avni. 2000. Molecular aspects of T-cell differentiation. *Br. Med. Bull.* 56: 969–984.
- Irizarry, R. A., C. Ladd-Acosta, B. Wen, Z. Wu, C. Montano, P. Onyango, H. Cui, K. Gabo, M. Rongione, M. Webster, et al. 2009. The human colon cancer methylome shows similar hypo- and hypermethylation at conserved tissue-specific CpG island shores. *Nat. Genet.* 41: 178–186.

34. Maunakea, A. K., R. P. Nagarajan, M. Bilenky, T. J. Ballinger, C. D'Souza, S. D. Fouse, B. E. Johnson, C. Hong, C. Nielsen, Y. Zhao, et al. 2010. Conserved role of intragenic DNA methylation in regulating alternative promoters. *Nature* 466: 253–257.
35. Kim, H. P., and W. J. Leonard. 2007. CREB/ATF-dependent T cell receptor-induced FoxP3 gene expression: a role for DNA methylation. *J. Exp. Med.* 204: 1543–1551.
36. Baron, U., S. Floess, G. Wieczorek, K. Baumann, A. Grützkau, J. Dong, A. Thiel, T. J. Boeld, P. Hoffmann, M. Edinger, et al. 2007. DNA demethylation in the human FOXP3 locus discriminates regulatory T cells from activated FOXP3(+) conventional T cells. *Eur. J. Immunol.* 37: 2378–2389.
37. Tsuji-Takayama, K., M. Suzuki, M. Yamamoto, A. Harashima, A. Okochi, T. Otani, T. Inoue, A. Sugimoto, T. Toraya, M. Takeuchi, et al. 2008. The production of IL-10 by human regulatory T cells is enhanced by IL-2 through a STAT5-responsive intronic enhancer in the IL-10 locus. *J. Immunol.* 181: 3897–3905.
38. Lai, A. Y., M. Fatemi, A. Dhasarathy, C. Malone, S. E. Sobol, C. Geigerman, D. L. Jaye, D. Mav, R. Shah, L. Li, and P. A. Wade. 2010. DNA methylation prevents CTCF-mediated silencing of the oncogene BCL6 in B cell lymphomas. *J. Exp. Med.* 207: 1939–1950.
39. Janson, P. C., L. B. Linton, E. A. Bergman, P. Marits, M. Eberhardson, F. Piehl, V. Malmström, and O. Winqvist. 2011. Profiling of CD4+ T cells with epigenetic immune lineage analysis. *J. Immunol.* 186: 92–102.
40. Luo, Y., X. Zhang, M. Zhao, and Q. Lu. 2009. DNA demethylation of the perforin promoter in CD4(+) T cells from patients with subacute cutaneous lupus erythematosus. *J. Dermatol. Sci.* 56: 33–36.
41. Jeffries, M., M. Dozmorov, Y. Tang, J. T. Merrill, J. D. Wren, and A. H. Sawalha. 2011. Genome-wide DNA methylation patterns in CD4+ T cells from patients with systemic lupus erythematosus. *Epigenetics* 6: 593–601.
42. Kim, H. R., K. A. Hwang, K. C. Kim, and I. Kang. 2007. Down-regulation of IL-7Ralpha expression in human T cells via DNA methylation. *J. Immunol.* 178: 5473–5479.
43. Nakajima, S., T. Honda, D. Sakata, G. Egawa, H. Tanizaki, A. Otsuka, C. S. Moniaga, T. Watanabe, Y. Miyachi, S. Narumiya, and K. Kabashima. 2010. Prostaglandin I2-IP signaling promotes Th1 differentiation in a mouse model of contact hypersensitivity. *J. Immunol.* 184: 5595–5603.
44. Tokoyoda, K., S. Zehentmeier, A. N. Hegazy, I. Albrecht, J. R. Grün, M. Löhning, and A. Radbruch. 2009. Professional memory CD4+ T lymphocytes preferentially reside and rest in the bone marrow. *Immunity* 30: 721–730.
45. Chetoui, N., M. Boisvert, S. Gendron, and F. Aoudjit. 2010. Interleukin-7 promotes the survival of human CD4+ effector/memory T cells by up-regulating Bcl-2 proteins and activating the JAK/STAT signalling pathway. *Immunology* 130: 418–426.
46. Yin, L. 2005. Chondroitin synthase 1 is a key molecule in myeloma cell-osteoclast interactions. *J. Biol. Chem.* 280: 15666–15672.
47. DeNucci, C. C., and Y. Shimizu. 2011. β 1 integrin is critical for the maintenance of antigen-specific CD4 T cells in the bone marrow but not long-term immunological memory. *J. Immunol.* 186: 4019–4026.
48. Li, S., S. Chen, X. Xu, A. Sundstedt, K. M. Paulsson, P. Anderson, S. Karlsson, H. O. Sjögren, and P. Wang. 2000. Cytokine-induced Src homology 2 protein (CIS) promotes T cell receptor-mediated proliferation and prolongs survival of activated T cells. *J. Exp. Med.* 191: 985–994.
49. Nakajima, Y., I. Tsuge, Y. Kondo, R. Komatsubara, N. Hirata, M. Kakami, M. Kato, H. Kurahashi, A. Urisu, and Y. Asano. 2008. Up-regulated cytokine-inducible SH2-containing protein expression in allergen-stimulated T cells from hen's egg-allergic patients. *Clin. Exp. Allergy* 38: 1499–1506.
50. Khor, C. C., F. O. Vannberg, S. J. Chapman, H. Guo, S. H. Wong, A. J. Walley, D. Vukcevic, A. Rautanen, T. C. Mills, K. C. Chang, et al. 2010. CISH and susceptibility to infectious diseases. *N. Engl. J. Med.* 362: 2092–2101.

A Clonogenic Progenitor with Prominent Plasmacytoid Dendritic Cell Developmental Potential

Nobuyuki Onai,^{1,2} Kazutaka Kurabayashi,¹ Mayuka Hosoi-Amaike,¹ Noriko Toyama-Sorimachi,³ Kouji Matsushima,^{2,4} Kayo Inaba,^{2,5} and Toshiaki Ohteki^{1,2,*}

¹Department of Biodefense Research, Medical Research Institute, Tokyo Medical and Dental University, Tokyo 113-8510, Japan

²Japan Science and Technology Agency, Core Research for Evolutional Science and Technology (CREST), Tokyo 102-0081, Japan

³Department of Molecular Immunology and Inflammation, Research Institute, National Center of Global Health and Medicine, Tokyo 162-8655, Japan

⁴Department of Molecular Preventive Medicine, Graduate School of Medicine, The University of Tokyo, Tokyo 113-0033, Japan

⁵Laboratory of Immunobiology, Department of Animal Development and Physiology, Division of Systemic Life Science, Graduate School of Biostudies, Kyoto University, Kyoto 606-8501, Japan

*Correspondence: ohteki.bre@mri.tmd.ac.jp

<http://dx.doi.org/10.1016/j.immuni.2013.04.006>

SUMMARY

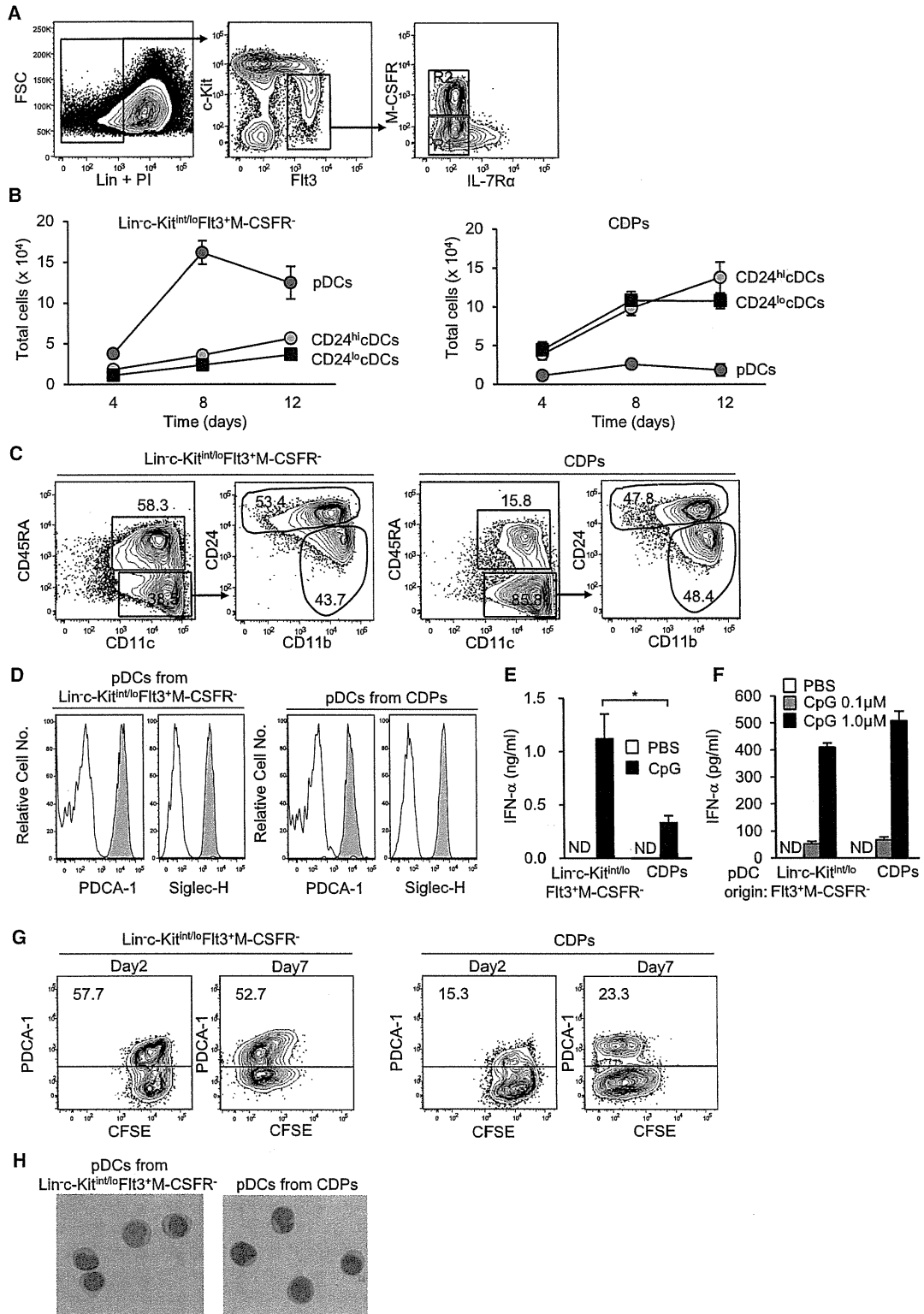
Macrophage and dendritic cell (DC) progenitors (MDPs) and common DC progenitors (CDPs) are bone marrow (BM) progenitors with DC differentiation potential. However, both MDPs and CDPs give rise to large numbers of conventional DCs (cDCs) and few plasmacytoid DCs (pDCs), implying that more dedicated pDC progenitors remain to be identified. Here we have described DC progenitors with a prominent pDC differentiation potential. Although both MDPs and CDPs express the macrophage colony stimulating factor (M-CSF) receptor (M-CSFR), the progenitors were confined to a M-CSFR⁻ fraction, identified as Lin⁻c-Kit^{int/lo}Flt3⁺M-CSFR⁻, and expressed high amounts of *E2-2* (also known as *Tcf4*) an essential transcription factor for pDC development. Importantly, they appeared to be directly derived from either CDPs or lymphoid-primed multipotent progenitors (LMPPs). Collectively, our findings provide insight into DC differentiation pathways and may lead to progenitor-based therapeutic applications for infection and autoimmune disease.

INTRODUCTION

Dendritic cells (DCs) have crucial functions in the initiation of innate and adaptive immunity in infection and inflammation and in the induction of tolerance under steady-state conditions (Banchereau and Steinman, 1998). DCs consist of conventional DCs (cDCs) and plasmacytoid DCs (pDCs) (Banchereau and Steinman, 1998; Liu, 2005; Shortman and Naik, 2007; Geissmann et al., 2010; Swiecki and Colonna, 2010). pDCs are present in human (Siegal et al., 1999; Cella et al., 1999) and mouse (Asselin-Paturel et al., 2001; Nakano et al., 2001; Björck, 2001) and are characterized by their capacity to produce large amounts of type I interferons (IFNs) (Siegal et al., 1999; Cella et al., 1999; Asselin-Paturel et al., 2001; Nakano et al., 2001; Björck, 2001). The pDCs' activation and type I IFN production

are critical for the initiation of antiviral immune responses, whereas pDCs' activation in the absence of infection causes autoimmune diseases, such as systemic lupus erythematosus (SLE) and psoriasis vulgaris (Gilliet et al., 2008; Banchereau and Pascual, 2006). In addition, local microenvironments can induce tolerogenic properties in pDCs (de Heer et al., 2004; Goubier et al., 2008). It was recently shown that basic helix-loop-helix transcription factor *E2-2* (also known as *TCF4*) is essential for pDC development in both human and mouse (Nagasawa et al., 2008; Cisse et al., 2008) and maintenance of mature pDCs (Ghosh, et al., 2010).

DCs are originated from hematopoietic stem cells (HSCs) in the bone marrow (BM) via intermediate progenitors (Shortman and Naik, 2007; Geissmann et al., 2010; Merad and Manz, 2009). The intermediate sequential progenitors are classified on the basis of their chemokine and cytokine receptor expression and in vivo DC differentiation ability (Fogg et al., 2006; Auffray et al., 2009; Liu et al., 2009; Onai et al., 2007; Naik et al., 2007). *Fms*-like tyrosine kinase receptor-3 (*Flt3*) has a nonredundant role in the steady-state differentiation and maintenance of pDCs and cDCs in vivo. Mice deficient for *Flt3* or *Flt3*-ligand (*Flt3L*) are poor producers of cDCs and pDCs in vivo (McKenna et al., 2000; Waskow et al., 2008), and the recently identified macrophage and DC progenitors (MDPs) and common DC progenitors (CDPs) express *Flt3* on their cell surface (Cisse et al., 2008; Fogg et al., 2006; Auffray et al., 2009; Liu et al., 2009). MDPs express the phenotypic markers Lin⁻CX₃CR1⁺CD11b⁻c-Kit⁺Flt3⁺M-CSFR⁺ and produce macrophages and cDCs and pDCs through CDPs (Fogg et al., 2006; Onai et al., 2007; Naik et al., 2007; Auffray et al., 2009; Liu et al., 2009), whereas CDPs are Lin⁻c-Kit^{int/lo}Flt3⁺M-CSFR⁺ cells that give rise exclusively to cDCs and pDCs (Onai et al., 2007; Naik et al., 2007), suggesting that CDPs are stringently committed to the DC lineage. The immediate cDC precursors, namely pre-DCs, which are derived from CDPs, migrate into lymphoid and some nonlymphoid tissues where they differentiate into cDCs (Naik et al., 2006, 2007; Varol et al., 2009; Bogunovic et al., 2009; Ginhoux et al., 2009). Notably, both MDPs and CDPs give rise to many fewer pDCs than cDCs. In this study, we identified DC-committed progenitors, i.e., Lin⁻c-Kit^{int/lo}Flt3⁺M-CSFR⁻IL-7R α ⁻ cells, with prominent pDC differentiation potential, and our findings revise the current understanding of DC differentiation pathways.



(legend on next page)

RESULTS

Identification of M-CSFR⁻ DC Progenitors

Because the MDPs and CDPs express M-CSFR, we initially examined whether DC developmental potential was exclusive to the M-CSFR⁺ fraction of Lin⁻ BM cells (Figure S1 available online). Lin⁻ BM cells were divided into four populations in terms of their c-Kit and M-CSFR expression: c-Kit^{hi}M-CSFR⁻ (R1), c-Kit⁺M-CSFR⁺ (R2), c-Kit^{int/lo}M-CSFR⁺ (R3), and c-Kit^{int/lo}M-CSFR⁻ (R4) cells (Figure S1A). R1 contained HSCs, multipotent progenitors (MPPs), and myeloid progenitors (MPs), and R2–R4 included MDPs (R2), CDPs (R3), and B cell progenitors (R4), respectively. In the presence of M-CSF, about 50% of R2 and a few percent of R1 and R3 gave rise to macrophage colonies, but R4 did not give rise to any macrophage colonies (Figure S1B).

To examine the DC differentiation potential of each fraction, we cultured the cells *ex vivo* in the presence of Flt3L for 8 days. Not only the Lin⁻M-CSFR⁺ fractions (R2 and R3), which include the MDPs and CDPs (Fogg et al., 2006; Onai et al., 2007; Naik et al., 2007), but also the Lin⁻M-CSFR⁻ fractions (R1 and R4) showed DC differentiation potential (Figures S1C and S1D). Among the latter fractions, we expected the c-Kit^{hi}M-CSFR⁻ cells (R1) to give rise to DCs, because this population contains the HSCs, MPPs, and MPs. The development of DCs from c-Kit^{int/lo}M-CSFR⁻ (R4) cells was unexpected, but these cells had a relatively stronger pDC differentiation potential (Figures S1C and S1D). Because only Lin⁻Flt3⁺ cells have DC differentiation potential (D'Amico and Wu, 2003; Karsunky et al., 2003), we focused on Lin⁻c-Kit^{int/lo}Flt3⁺M-CSFR⁻ cells as a likely population for the pDC precursors; we also excluded the interleukin-7 receptor α chain-positive (IL-7R α ⁺) cells from the Lin⁻c-Kit^{int/lo}Flt3⁺M-CSFR⁻ fraction (hereafter, Lin⁻c-Kit^{int/lo}Flt3⁺M-CSFR⁻ cells), because this population contains B cell progenitors (Figure 1A; Onai et al., 2007). The proportion of Lin⁻c-Kit^{int/lo}Flt3⁺M-CSFR⁻ cells was 0.1% in the whole BM cells and the ratio of Lin⁻c-Kit^{int/lo}Flt3⁺M-CSFR⁻ cells (R1) and CDPs (R2) was 1:1 (Figure 1A).

To evaluate the DC developmental potential of the Lin⁻c-Kit^{int/lo}Flt3⁺M-CSFR⁻ cells in comparison with CDPs *ex vivo*, we cultured 2×10^4 Lin⁻c-Kit^{int/lo}Flt3⁺M-CSFR⁻ cells and CDPs in Flt3L-supplemented medium for 4, 8, and 12 days

(Figure 1B). On day 8, when the number of pDCs reached its peak, the Lin⁻c-Kit^{int/lo}Flt3⁺M-CSFR⁻ cells gave rise exclusively to DCs, and the majority of their progeny were pDCs (CD45RA⁺CD11c^{int}); the rest were cDCs (CD45RA⁻CD11c⁺) containing both the CD11b^{lo}CD24^{hi} and CD11b^{hi}CD24^{lo} subpopulations (Figures 1B, left and 1C, left). As reported previously (Onai et al., 2007; Naik et al., 2007), CDPs gave rise to a large number of cDCs and a few pDCs (Figures 1B, right and 1C, right). On day 8, the absolute number of pDCs generated from Lin⁻c-Kit^{int/lo}Flt3⁺M-CSFR⁻ cells was 6–8 times higher than that from CDPs. However, CDPs produced 3- to 4.5-fold more cDC subsets (Figure 1B). The CD45RA⁺CD11c^{int} cells derived from Lin⁻c-Kit^{int/lo}Flt3⁺M-CSFR⁻ cells and CDPs expressed plasmacytoid dendritic cell antigen-1 (PDCA-1) and sialic acid binding Ig-like lectin (Siglec)-H, confirming that they were genuine pDCs (Figure 1D). As expected from the abundant pDCs, the progenies of Lin⁻c-Kit^{int/lo}Flt3⁺M-CSFR⁻ cells produced higher amounts of IFN- α than did those of CDPs after CpG stimulation (Figure 1E). Indeed, the same numbers of pDCs derived from Lin⁻c-Kit^{int/lo}Flt3⁺M-CSFR⁻ cells and CDPs produced IFN- α at comparable amounts upon CpG stimulation (Figures 1F). The Lin⁻c-Kit^{int/lo}Flt3⁺M-CSFR⁻ cells and CDPs showed similar proliferative potential *ex vivo* (Figure 1G), and the pDCs derived from the Lin⁻c-Kit^{int/lo}Flt3⁺M-CSFR⁻ cells had a typical pDC morphology (Figures 1H). From these results, we concluded that Lin⁻c-Kit^{int/lo}Flt3⁺M-CSFR⁻ cells are DC-committed progenitors with prominent pDC differentiation potential (hereafter, M-CSFR⁻ DC progenitors).

Under the same culture conditions, 1 of 8.6 M-CSFR⁻ DC progenitors (Figure 2A) and 1 of 7.1 CDPs (Figure 2B) gave rise to CD11c⁺ cells as estimated by limiting-dilution analysis. That is, 43 out of 183 single-sorted M-CSFR⁻ DC progenitors gave rise to CD11c⁺ cells, which included 22 clones generating only pDCs, 12 generating only cDCs, and 9 generating both pDCs and cDCs (Figure 2C). In the case of cDC-only colonies, some contained both CD11b^{hi}CD24^{lo} and CD11b^{lo}CD24^{hi} subpopulations, and some contained only one of them (Figure 2D). In the case of colonies that give rise to both cDCs and pDCs, the ratio of pDCs to cDCs varied (Figure 2E). The results of limiting-dilution analysis of M-CSFR⁻ DC progenitors (Figure 2F and CDPs (Figure 2G) were summarized as Venn diagrams, showing that

Figure 1. Identification of M-CSFR⁻ DC Progenitors

- (A) Flow cytometric sorting of BM Lin⁻ cells (left), those expressing Lin⁻c-Kit^{int/lo}Flt3⁺ (middle), and, of them, those expressing M-CSFR and IL-7R α (right). Boxed areas: R1, Lin⁻c-Kit^{int/lo}Flt3⁺M-CSFR⁻IL-7R α ⁻; R2, CDPs (Lin⁻c-Kit^{int/lo}Flt3⁺M-CSFR⁺).
- (B–E) *Ex vivo* DC differentiation from sorted Lin⁻c-Kit^{int/lo}Flt3⁺M-CSFR⁻IL-7R α ⁻ cells and CDPs.
- (B) Cells (2×10^4) were cultured in the presence of human Flt3L-Ig (100 ng/ml) and absolute numbers of pDC (CD45RA⁺CD11c^{int}) and cDC (CD24^{lo} cDCs and CD24^{hi} cDCs) subpopulations on day 4, 8, and 12 of culture.
- (C) Flow cytometric profiles of the DC subsets.
- (D) PDCA-1 or Siglec-H expression (shaded) and corresponding isotype controls (open) on pDCs.
- (E) IFN- α production (1 μ M CpG for 24 hr) on day 8 of culture.
- (F) On day 8 of culture, pDCs derived from Lin⁻c-Kit^{int/lo}Flt3⁺M-CSFR⁻IL-7R α ⁻ cells and CDPs were stimulated with CpG for 24 hr, and IFN- α activity in the culture supernatants was evaluated by ELISA.
- ND, not detected. Means \pm SEM are shown. n = 8 from five (A–D) or three (E, F) independent experiments.
- (G) Division-coupled differentiation into pDCs from Lin⁻c-Kit^{int/lo}Flt3⁺M-CSFR⁻IL-7R α ⁻ cells (left) and CDPs (right). DC progenitors were labeled with CFSE and cultured in the presence of hFlt3L-Ig (100 ng/ml) for 2 days and 7 days.
- (H) May-Grünwald-Giemsa staining of sorted pDCs derived from Lin⁻c-Kit^{int/lo}Flt3⁺M-CSFR⁻IL-7R α ⁻ cells (left) and CDPs (right). Original magnification, $\times 400$. Data are representative of three independent experiments.
- See also Figure S1.

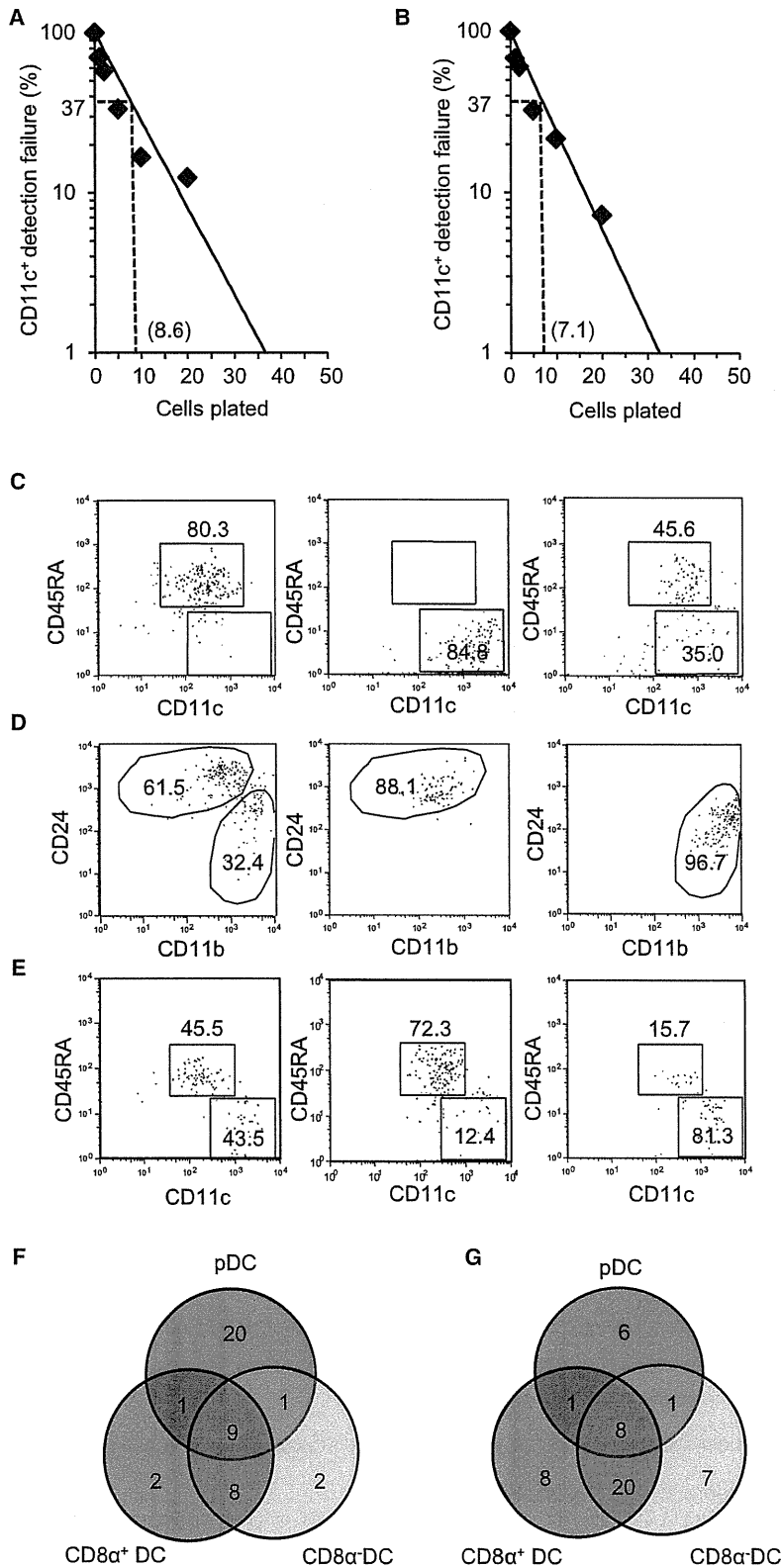


Figure 2. Limiting Dilution Analysis of M-CSFR⁻ DC Progenitors

(A and B) Limiting dilution analysis of M-CSFR⁻ DC progenitors (A) and CDPs (B). Cells were cultured for 12 days with Ac6 stromal cells and hFit3L-Ig (100 ng/ml); each well was analyzed for CD11c⁺ cells. Horizontal axis, number of plated cells. Dotted line, 37% negative “readout” showing the predicted frequency of CD11c⁺ progenitor cells in parentheses. Statistics details are described in Experimental Procedures.

(C) Clonal analysis of M-CSFR⁻ DC progenitors. Single progenitors gave rise to pDCs (left), cDCs (middle), or both (right).

(D) Subsets of cDCs defined as in Figure 1C.

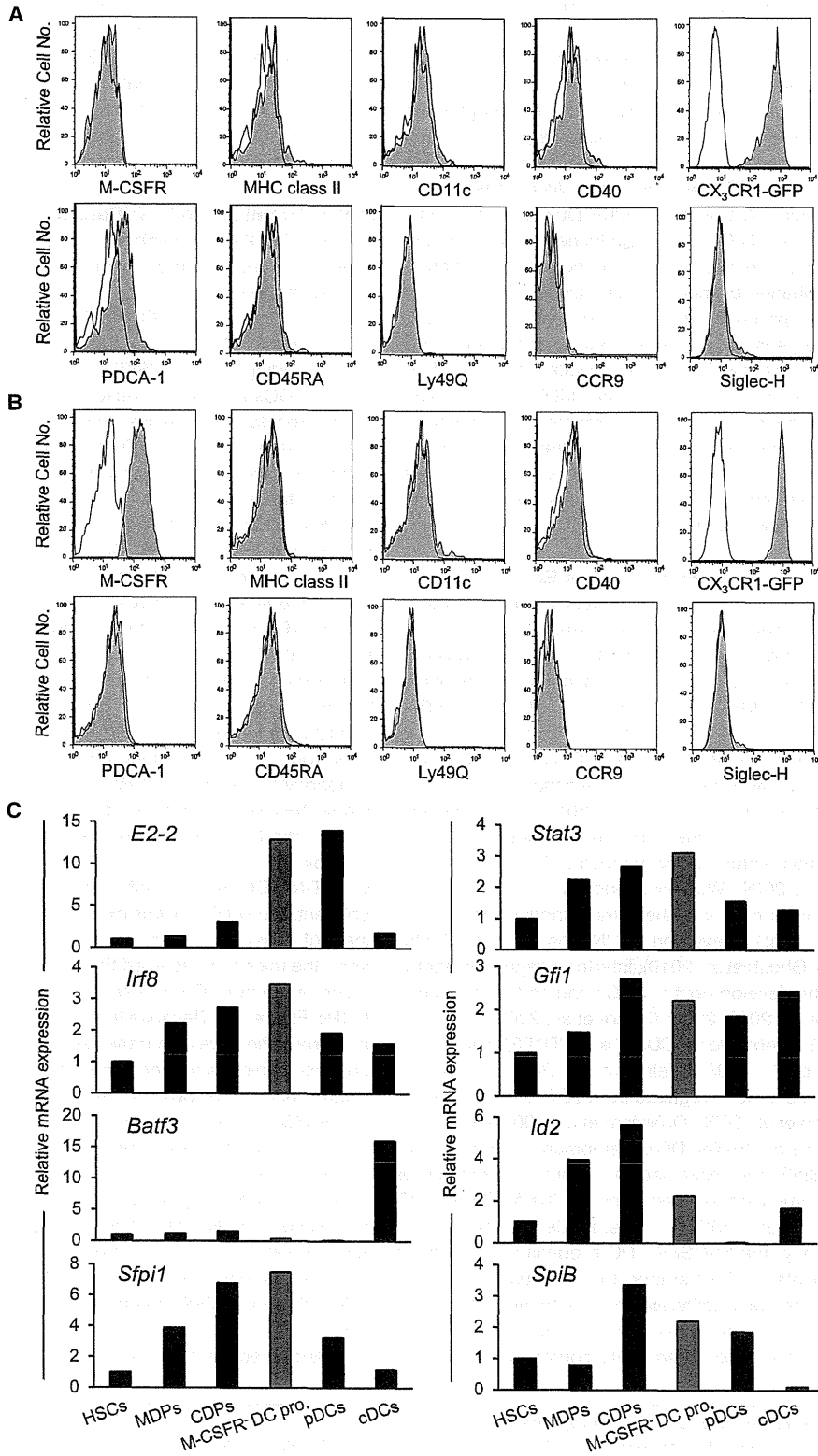
(E) Single bipotential progenitors gave rise to both pDCs and cDCs. Some clones gave rise to comparable numbers of pDCs and cDCs (left), some clones gave rise to a large number of pDCs and some cDCs (middle), and other clones gave rise to some pDCs and many cDCs (right). Data are representative of three independent experiments.

(F and G) Venn diagrams of the progenies of single M-CSFR⁻ DC progenitors (F) or CDPs (G) sorted and plated at a density of 1 cell per well in 96-well plates (for a total of 182 wells) on irradiated Ac6 stromal cells in human Fit3L-Ig-supplemented media. Values represent the number of wells on day 12 with cells of the indicated type. Data are combined from three independent experiments.

See also Figure S2.

Immunity

DC Progenitors Expressing High Amounts of *E2-2*



(legend on next page)

M-CSFR⁻ DC progenitors contain more clones that give rise to pDCs.

To further ensure DC-committed differentiation potential of M-CSFR⁻ DC progenitors, we examined the myelo-erythroid and B cell differentiation potential of M-CSFR⁻ DC progenitors by using ex vivo assays for colony-forming units (CFU) (Figures S2A–S2C). For comparison, Lin⁻c-Kit^{int}Sca-1⁺ cells, which are a mixture of HSCs and MPPs, were included. As reported previously (Fogg et al., 2006; Auffray et al., 2009; Liu et al., 2009; Onai et al., 2007; Naik et al., 2007), MDPs contained colony-forming activities for myeloid lineages, resulting in colonies of granulocytes and macrophages or macrophages alone, but less than 3% of the CDPs produced myeloid colonies. In contrast, M-CSFR⁻ DC progenitors contained few macrophage CFU and completely lacked CFU for other myeloid lineages (Figure S2A). Furthermore, compared with MDPs, CDPs and M-CSFR⁻ DC progenitors produced few macrophage colonies, and neither of them produced pre-B cells (Figures S2B and S2C). Therefore, we concluded that M-CSFR⁻ DC progenitors have minimal myeloid differentiation potential and lack erythroid and pre-B cell differentiation potential.

M-CSFR⁻ DC Progenitors Highly Express *E2-2*

We further characterized in detail the molecular phenotypes of the M-CSFR⁻ DC progenitors. First we examined their expression of cell surface molecules and found that they were positive for CX₃CR1, expressed PDCA-1 at minimal amounts, and were negative for M-CSFR, MHC class II, CD11c, CD40, CD45RA, Ly49Q, CCR9, and Siglec-H (Figure 3A). In this context, CDPs expressed M-CSFR but never expressed PDCA-1 (Figure 3B). In addition, DNA microarray analysis revealed that the M-CSFR⁻ DC progenitors did not distinctly express other surface markers including receptors for cytokines and chemokines (Table S1). Several transcription factors critically regulate DC development (Merad and Manz, 2009; Watowich and Liu, 2010; Belz and Nutt, 2012): the basic helix-loop-helix transcription factor *E2-2* specifically controls pDC development (Nagasawa et al., 2008; Cisse et al., 2008; Ghosh et al., 2010), interferon regulatory factor 8 (IRF) controls the development of pDCs and certain cDC subsets (Schiavoni et al., 2002, 2004; Aliberti et al., 2003; Tsujimura et al., 2003), *Batf3* is required for CD8 α ⁺ and CD103⁺ cDC development (Hildner et al., 2008; Edelson et al., 2010), and *PU.1*, encoded by *Sfp1*, seems to regulate both cDC and pDC development (Anderson et al., 2000; Guerriero et al., 2000; Onai et al., 2006). Other factors controlling DC development include *STAT3*, *Gfi-1*, *Id2*, and *Sp1B*. We examined the expression profiles of these DC development-associated genes in the M-CSFR⁻ DC progenitors and in HSCs, MDPs, CDPs, pDCs, and cDCs (Figure 3C). Importantly, the M-CSFR⁻ DC progenitors expressed the highest amounts of *E2-2* among those tested, consistent with their prominent pDC differentiation potential. They also expressed critical DC lineage-associated genes, such as *Irf8*, *Sfp1*, *Stat3*, *Gfi1*, and *Sp1B* at amounts comparable to CDPs,

and *Id2* at lower amounts than the other DC progenitors, confirming their DC developmental potential. In contrast, *Batf3* expression in the M-CSFR⁻ DC progenitors was negligible. These results indicated that the molecular phenotypes of the M-CSFR⁻ DC progenitors are suitable for DC progenitors and the highest amounts of *E2-2* expression is consistent with their prominent pDC differentiation potential.

In Vivo Prominent pDC Differentiation Potential of M-CSFR⁻ DC Progenitors

To evaluate the in vivo differentiation potential of the M-CSFR⁻ DC progenitors, 5 × 10⁴ M-CSFR⁻ DC progenitors or CDPs from B6 mice (CD45.1⁻CD45.2⁺) were injected into irradiated B6.SJL mice (CD45.1⁺CD45.2⁻) (Figure 4). In line with our ex vivo findings, the M-CSFR⁻ DC progenitors gave rise exclusively to DCs and not to lineages including T, B, and NK cells, or erythrocytes in the spleen and BM of the progenitor-injected mice (Figures 4A and 4B). Furthermore, 10 days after the transplantation, when the number of progeny cells peaked (Figure 4C), most of the M-CSFR⁻ DC progenitors' progenies were pDCs (CD45RA⁺CD11c^{int}) in these organs, which expressed additional pDC markers, including PDCA-1 and Siglec-H (Figures 4A and 4B). Compared with CDPs, the M-CSFR⁻ DC progenitors gave rise to 5–6 times more pDCs, but only 1/3 the number of cDCs (Figure 4D). In addition, the M-CSFR⁻ DC progenitor-derived pDCs and cDCs expressed normal amounts of Toll-like receptor 7 (TLR7) and TLR9 and of TLR2 and TLR4, respectively (Figures 4E and S3A); the pDCs were capable of producing robust IFN- α in response to CpG stimulation ex vivo (Figure 4F); and the cDCs effectively induced T cell proliferation in allogeneic mixed lymphocyte reactions (MLRs) (Figure S3B). To further demonstrate the biological relevance of the M-CSFR⁻ DC progenitors in vivo, the M-CSFR⁻ DC progenitors, MDPs, and CDPs were transplanted into irradiated mice. Ten days after transplantation, CpG DNA⁺DOTAP was intravenously injected, and the serum concentration of IFN- α was examined. Consistent with the prominent pDC developmental potential of the M-CSFR⁻ DC progenitors, the mice that received these cells produced a significantly higher amount of IFN- α than those transplanted with MDPs or CDPs (Figure 4G). Because the LNs became too small to analyze after irradiation, we also transplanted the M-CSFR⁻ DC progenitors into nonirradiated recipients and noted that they gave rise to a large number of pDCs in the spleen, LNs, and BM (Figures S3C–S3G). Of note, the progenies were mostly pDCs in the BM, which is consistent with a previous report showing that pDCs are abundantly present in the BM under steady-state conditions (Zhang et al., 2006). In addition, the M-CSFR⁻ DC progenitor-derived pDCs contained a larger number of CCR9⁻ subpopulation in the BM than those in the spleen (Figures S3E). To further examine whether DC progenitors give rise to pDCs through CCR9⁻ intermediate precursors (Schlitzer et al., 2011), we cultured 2 × 10⁴ M-CSFR⁻ DC progenitors in Flt3L-supplemented medium for 2 or 4 days (Figure S3H). The

Figure 3. Characterization of M-CSFR⁻ DC Progenitors

(A and B) Histograms showing surface markers of M-CSFR⁻ DC progenitors (A) and CDPs (B). Shaded areas, indicated molecules; open areas, corresponding isotype controls.

(C) RNAs for DC lineage-associated genes were analyzed by qPCR in HSCs, MDPs, CDPs, M-CSFR⁻ DC progenitors, pDCs, and cDCs. Data are representative of three independent experiments. See also Table S1.